# Trans-Blood Brain Barrier Delivery of Dopamine-Loaded Nanoparticles Reverses Functional Deficits in Parkinsonian Rats

**Richa Pahuja,[†,‡,§,#] Kavita Seth,[*,†,#] Anshi Shukla,[†] Rajendra Kumar Shukla,[†] Priyanka Bhatnagar,[‡] Lalit Kumar Singh Chauhan,[†] Prem Narain Saxena,[†] Jharna Arun,[∥] Bhushan Pradosh Chaudhari,[†,§] Devendra Kumar Patel,[†,§] Sheelendra Pratap Singh,[†] Rakesh Shukla,[§,∥] Vinay Kumar Khanna,[†,§] Pradeep Kumar,[‡,§] Rajnish Kumar Chaturvedi,[*,†,§] and Kailash Chand Gupta[*,†,‡,§,⊥]**

[†]CSIR-Indian Institute of Toxicology Research (CSIR-IITR), 80 MG Marg, Lucknow 226001, India, [‡]CSIR-Institute of Genomics & Integrative Biology (CSIR-IGIB), Mall Road, Delhi 110007, India, [§]Academy of Scientific and Innovative Research (AcSIR), Delhi 110001, India, and [∥]CSIR-Central Drug Research Institute (CSIR-CDRI), Lucknow 226001, India. [#]R. Pahuja and K. Seth contributed equally to this work. [⊥]Present address: CSIR-Institute of Genomics & Integrative Biology (CSIR-IGIB), Mall Road, Delhi 110007, India.

**ABSTRACT** Sustained and safe delivery of dopamine across the blood brain barrier (BBB) is a major hurdle for successful therapy in Parkinson's disease (PD), a neurodegenerative disorder. Therefore, in the present study we designed neurotransmitter dopamine-loaded PLGA nanoparticles (DA NPs) to deliver dopamine to the brain. These nanoparticles slowly and constantly released dopamine, showed reduced clearance of dopamine in plasma, reduced quinone adduct formation, and decreased dopamine autoxidation. DA NPs were internalized in dopaminergic SH-SY5Y cells and dopaminergic neurons in the substantia nigra and striatum, regions affected in PD. Treatment with DA NPs did not cause reduction in cell viability and morphological deterioration in SH-SY5Y, as compared to bulk dopamine-treated cells, which showed reduced viability. Herein, we report that these NPs were able to cross the BBB and capillary endothelium in the striatum and substantia nigra in a 6-hydroxydopamine (6-OHDA)-induced rat model of PD. Systemic intravenous administration of DA NPs caused significantly increased levels of dopamine and its metabolites and reduced dopamine-D2 receptor supersensitivity in the striatum of parkinsonian rats. Further, DA NPs significantly recovered neurobehavioral abnormalities in 6-OHDA-induced parkinsonian rats. Dopamine delivered through NPs did not cause additional generation of ROS, dopaminergic neuron degeneration, and ultrastructural changes in the striatum and substantia nigra as compared to 6-OHDA-lesioned rats. Interestingly, dopamine delivery through nanoformulation neither caused alterations in the heart rate and blood pressure nor showed any abrupt pathological change in the brain and other peripheral organs. These results suggest that NPs delivered dopamine into the brain, reduced dopamine autoxidation-mediated toxicity, and ultimately reversed neurochemical and neurobehavioral deficits in parkinsonian rats.

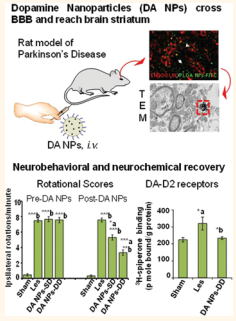


**KEYWORDS:** nanoparticles · dopamine · Parkinson's disease · tyrosine hydroxylase

Polymeric drug delivery systems have been widely developed and provide an attractive alternative for long-term delivery of otherwise blood brain barrier (BBB) impermeable therapeutic agents to the brain.[1−3] Dopamine is one such molecule, the deficiency of which is a key feature of neurodegenerative Parkinson's disease (PD), which becomes gradually worse over time.[4] The reason for dopamine loss is progressive decay of a substantial proportion of dopamine-synthesizing neurons in the substantia nigra. The human brain has ~600 000 dopaminergic neurons comprising 1% of the total CNS neuronal number. The somatodendritic part of these neurons resides in the substantia nigra, synthesizing the neurotransmitter dopamine, while their axonal projections are extended to the striatal region.[5] Tonic firing pumps dopamine from the nigra to the striatum, an essential mechanism to maintain striatonigral dopaminergic circuitry, which accounts for most of the body movements. The death of dopaminergic neurons obstructs the supply of the neurotransmitter dopamine to the brain striatum, resulting in uncontrolled behavioral deficits and gait imbalance.[6] The disease

* Address correspondence to rajnish@iitr.res.in, sethkavita@rediffmail.com, kcgupta@iitr.res.in.

Received for review November 10, 2014 and accepted March 31, 2015.

**Published online March 31, 2015**
**10.1021/nn506408v**

symptoms are severe and precipitate only after substantial degeneration (>80%) of dopamine neurons has taken place.[7] The ultimate effective approach to relieve the disease symptoms is replenishment of missing dopamine on a day-to-day basis. As a proof of principle, direct dopamine infusion into the brain of PD animal models is reported to curtail the behavioral abnormalities imparting symptomatic relief.[8−10] As dopamine does not cross the BBB and direct dopamine infusion into the brain is not possible in human subjects, the clinical management of PD is done through frontline drugs including the dopamine precursor L-DOPA (L-3,4-dihydroxyphenylalanine), dopamine receptor agonists, inhibitors targeting dopamine-degrading catechol-*o*-methyltransferase, and monoamine oxidase B, alone or in combination.[11−13] However, these drugs are not without side effects, with the most prominent being dyskinesia and wearing-off effects. On chronic use in advanced disease conditions, these drugs become ineffective. Further, the capacity of dopamine storage cells to retain dopamine delivered by the medication is also impaired. In addition, loss of dopa decarboxylase enzyme involved in conversion of L-DOPA to dopamine compromises the therapeutic efficacy of the drug.[14] Often a stage is reached where side effects of the drugs outweigh their therapeutic benefits, leaving the patients in an unmanageable disease state.

A novel approach is to use dopamine itself by making it cross the BBB in the form of dopamine-loaded polymeric nanoparticles (DA NPs). DA NPs may offer several advantages for dopamine delivery into the brain. Entrapment of dopamine within a polymeric matrix may help its delivery in the brain in a sustained and continuous fashion, without significant peripheral metabolism. This may reduce the need for repeated drug administration, cutting down peripheral and central toxicity. Interestingly, the small size of NPs may make them compatible with various administration routes including intravenous (iv) injection.

Keeping these in mind, in the present study, we prepared dopamine-encapsulated poly(lactic-*co*-glycolic acid) (PLGA) NPs, capable of slow and sustained release of dopamine. PLGA was used due to its biodegradable, biocompatible properties and versatile degradation kinetics. PLGA has been successfully used as a delivery vehicle for several pharmacological molecules in the brain.[15−18] In the present study, we demonstrated that PLGA NPs mediated dopamine delivery in the brain through systemic iv infusion in a 6-hydroxydopamine (6-OHDA)-induced rat model of PD. We found that DA NPs crossed the BBB and internalized into the brain. We further tested their potential in restoring neurobehavioral and neurochemical deficits in parkinsonian rats. These particles up-regulated and maintained the dopamine levels in the lesioned striatum through slow and sustained release. This was accompanied by a decrease in dopamine receptor supersensitivity and reversal of neurobehavioral deficits. We further observed no detrimental cardiovascular and free radical toxicity. We hope this approach after further validation can be used for safe and effective systemic delivery of dopamine.

## RESULTS AND DISCUSSION

**Preparation and Characterization of DA NPs and *In Vitro* Release Profile.** Continuous and slow delivery of dopamine, its precursor L-DOPA, or dopamine agonist in the brain is a must in order to minimize motor complications and drug-induced dyskinesia in PD.[19−21] Therefore, in the present study we prepared a nanoformulation of anti-Parkinson's neurotransmitter dopamine entrapped in a PLGA polymer to enable its systemic delivery to the brain. Dopamine present in the blood is restricted from entering the brain because of low lipid solubility and lack of specific transport carriers in the luminal membrane of the capillary endothelial cells, which constitute a major part of the BBB. Reports related to direct delivery of dopamine into the brain, through implantation of dopamine-loaded biodegradable hydrogel or a titanium oxide−dopamine complex or even through an infusion pump had shown its usefulness in attenuating behavioral abnormalities in parkinsonian rats.[9,10,22] Similarly, viral vector-mediated continuous delivery of L-DOPA reversed behavioral deficits in a rodent model of PD and L-DOPA-induced dyskinesia.[20] However, all these types of delivery methods involve surgical intervention and are not feasible for long-term delivery of dopamine in the brain.

To start with the formulation, the initial step was to select a suitable vehicle to deliver dopamine into the brain. Previously, we successfully delivered curcumin to the brain hippocampus through PLGA. Therefore, we selected PLGA to deliver dopamine into the brain.[23] Other reports also support the capability of PLGA in trans-CNS delivery of different drugs/therapeutic molecules in models of neurodegenerative disorders.[24−26] Our recent study suggested that PLGA-encapsulated nicotine significantly enhanced functional recovery in a rodent model of PD.[25] Similarly, use of PLGA as a delivery vehicle provided constant and sustained release of two therapeutic neurotrophic factors, namely, glial cell line-derived neurotrophic factor (GDNF) and vascular endothelial growth factor (VEGF) in a 6-OHDA-induced rat model of PD.[27] Another reason for using PLGA as an entrapment agent was to minimize many concerns regarding the fate of the NP matrix inside the brain. PLGA is biodegradable and biocompatible, and its degradation products lactic acid and glycolic acid are eliminated as carbon dioxide and water *via* the Krebs cycle.

We then targeted at evading rapid clearance of dopamine from the blood. Dopamine has a very short plasma half-life (~2 min) and undergoes metabolism

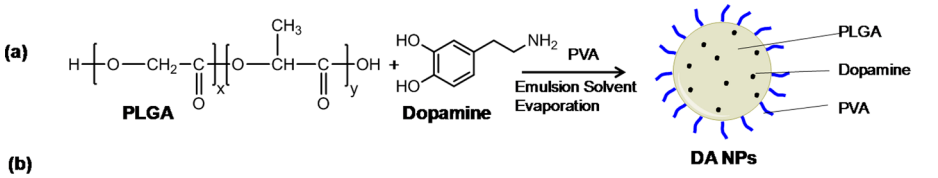


(b)

| Formulation | Size (nm) | PDI | ξ (mV) | EE (%) | LE (%) |
|---|---|---|---|---|---|
| PLGA NPs | 167.00 ± 17.20 | 0.230 ± 0.130 | - 19.100 ± 0.566 | - | - |
| DA NPs | 119.70 ± 2.69 | 0.104 ± 0.040 | - 2.660 ± 0.036 | 35.55 | 11.85 |
| PLGA NPs-FITC | 156.70 ± 2.28 | 0.145 ± 0.090 | - 14.700 ± 0.747 | - | - |

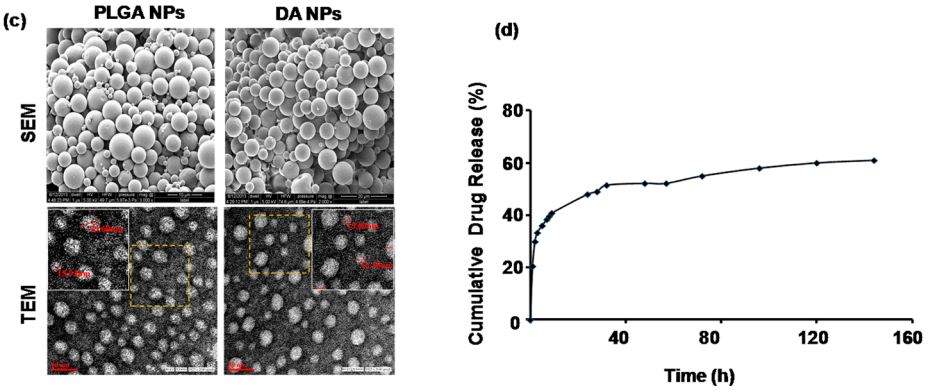


**Figure 1. Synthesis and characterization of nanoparticles: (a) Schematic representation of the synthesis of DA NPs. PLGA is emulsified with dopamine and PVA and assembles to give DA NPs by the emulsion solvent evaporation method. (b) Size, polydispersity index (PDI), and zeta-potential (ξ) of PLGA (PLGA NPs), dopamine-encapsulated PLGA (DA NPs), and FITC-linked PLGA nanoparticles (PLGA NPs-FITC) as measured through dynamic laser light scattering. Entrapment and loading efficiencies of dopamine in DA NPs were measured through spectrophotometry. (c) Photomicrographs of PLGA NPs and DA NPs taken through a scanning electron microscope (SEM), and TEM depicts their smooth spherical morphology. Scale bar: 10 and 20 $\mu$m for SEM and 50 nm for TEM. Inset of the marked area in yellow shows particle size. (d) Graph showing *in vitro* release kinetics of dopamine from DA NPs as percent drug release.**

by neurotransmitter amine metabolizing enzymes present in the peripheral circulation.[28] Since maintenance of prolonged and sufficient levels of dopamine in circulation (plasma) was mandatory to increase its chances to enter the brain, we preferred matrix-entrapped dopamine rather than surface adsorbed. Entrapment of dopamine in PLGA significantly enhanced the retention time of dopamine, as evident from our results. Encapsulation of dopamine not only protected it from rapid peripheral metabolism but also enabled its slow and sustained release. This also favored the decreased plasma load of oxidative metabolites of dopamine, leading to decreased toxicity, as evident in our subsequent experiments.

Unloaded control PLGA nanoparticles (PLGA NPs), dopamine-loaded (DA NPs), and FITC-linked PLGA NPs (PLGA NPs-FITC) were prepared using the double emulsion solvent evaporation method. Dopamine was physically entrapped in the PLGA matrix in DA NPs, while the other two were not loaded with dopamine and used as controls. In the case of fluorescent labeled particles, FITC was chemically conjugated first to PLGA using EDAC/NHS chemistry followed by preparation of NPs using the emulsification−evaporation technique. Emulsifying polymer, poly(vinyl alcohol) (PVA), was added to stabilize the formulation, which led to the formation of NPs dispersible in aqueous media (Figures 1a and S1). We determined their particle size, zeta-potential, shape, entrapment and loading efficiencies, and release profile. The mean diameter and charge of PLGA NPs-FITC as measured by dynamic light scattering (DLS) were 156.7 ± 2.28 nm and −14.7 ± 0.747 mV, respectively (Figure 1b). The hydrodynamic diameter/particle size of DA NPs was 119.7 ± 2.69 nm, suggesting that the size of NPs was in nanometer range. DA NPs showed a surface charge (zeta potential) of −2.66 ± 0.036 mV, with a low polydispersity index (PDI) of 0.104 (Figure 1b). A low value of the PDI reflects the uniformity in size of our particles. The particle size in a therapeutic delivery system highly affects the pharmacokinetic parameters. A large deviation can cause irregularity in pharmacokinetics, its circulation, and distribution, and thus affect its therapeutic efficiency.[29] Control PLGA NPs exhibited a size of 167.0 ± 17.20 nm and zeta potential of −19.1 ± 0.566 mV. The plausible reason for the difference in size of PLGA NPs and DA NPs could be their extent of hydration. DLS was performed in the hydrated state. In PLGA NPs more sites available in the polymer matrix can participate in hydration in comparison to DA NPs, where some of the sites are blocked by dopamine due to hydrophobic interactions and may not be available for the hydration process. In addition, the outward diffusion of dopamine in DA NPs probably further counteracted the

inflow of water into NPs. This probably led to the different swelling of two preparations, and thus hydrodynamic size estimates of PLGA NPs were higher in comparison to DA NPs, as a similar finding reported earlier.[30]

Transmission electron microscopy (TEM) analysis further confirmed the size to be in the nanometer range (Figure 1c); however it was less than that measured through DLS. The mean size of DA NPs and PLGA NPs as observed under TEM was 30 ± 5 nm and 22 ± 3 nm, respectively. This difference in values obtained from TEM and DLS can be attributed to the state of NPs used for measurement. TEM assessment was made using dry particles, and it measured the area of the sphere (core). On the other hand, DLS measurement was performed in a liquid suspension of NPs and hence measured the hydrodynamic size, which consisted of a particle core along with the solvent layer attached to the particle as it moves in the liquid under the influence of Brownian motion. An identical pattern of difference in the size estimated through TEM and DLS was also evident in our previous study.[23] TEM further depicted the spherical shape of these particles. Scanning electron microscopy (SEM) analysis confirmed the spherical appearance and smooth surface of NPs (Figure 1c). The entrapment and loading efficiencies of dopamine in NPs were 35.55 ± 5% and 11.85 ± 2%, respectively (Figure 1b). Thus, 1 mg of DA NPs carries around 118.5 μg of dopamine, which was reasonable considering the hydrophilic nature of dopamine.

The release kinetics of dopamine from the DA NPs was studied for 7 days in phosphate buffer saline (PBS) at 37 ± 2 °C, and we observed continuous dopamine release throughout this time. From the release graph it is evident that 60% of the encapsulated dopamine was released in 7 days (Figure 1d). The percent drug release was recorded to be fast initially. Thereafter, a prolonged sustained release phase with varying release rates was observed. Dopamine released from PLGA exhibited a typical biphasic pattern, with an initial burst (surface desorption, diffusion, and dissolution) followed by sustained release (bulk erosion due to diffusion of dopamine and degradation of the PLGA matrix). This suited our requirement, as the encapsulant polymer released the dopamine readily. A restricted release otherwise would have hindered the availability of the dopamine and may alter the drug efficacy. Earlier, a detailed review on PLGA-based drug delivery systems described a similar biphasic pattern of drug release, with an initial burst followed by a lag phase with a sustained liberation.[31] The initial burst was ascribed to the diffusion of the drug adsorbed on the surface, while the sustained pattern reportedly involved release of entrapped drug due to polymer matrix erosion along with diffusion.[32]

DA NPs and PLGA NPs-FITC were assessed for physical stability by suspending them in cell culture medium and measuring their size using DLS (Figure 2). Earlier a similar approach was followed by Lazzari *et al.*[33] to analyze poly(lactic acid) and poly(methyl methacrylate) NPs in different biological fluids. We observed that the initial hydrodynamic sizes of DA NPs and PLGA NPs-FITC in media were 124.3 ± 10.13 and 138.6 ± 19.7 nm, respectively. We did not observe any significant change in the hydrodynamic diameter of DA NPs and PLGA NPs-FITC until 24 h. On the basis of the above experiment, it can be stated that the particles used in the study remained stable during the test period. Wang *et al.*[34] examined the stability of doxorubicin- and paclitaxel-loaded PLGA NPs in PBS and did not notice any remarkable change in hydrodynamic size. Similar findings have been reported by others also.[35]

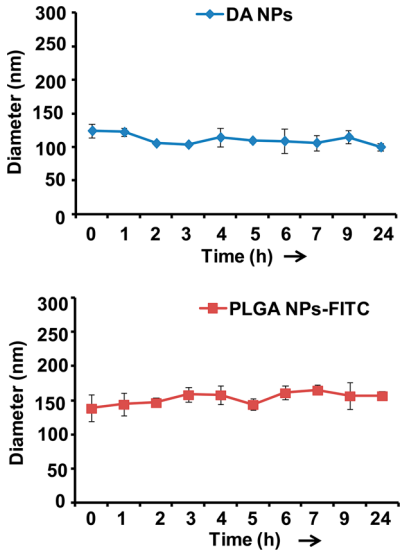


**Figure 2. Stability assessment of the nanoparticles: DA NPs and PLGA NPs-FITC were suspended in cell culture medium and incubated at 37 °C. DLS size measurements were made at 1 h intervals. There was no significant change in the sizes of the particles, and thus the particles showed stable behavior in the medium.**

**DA NPs Are Less Prone to Oxidation than Bulk Dopamine.** In order to demonstrate the stability of polymer-coated dopamine, we entrapped dopamine inside a polymeric compartment to protect it from oxidative damage and expected lesser oxidation of DA NPs in comparison to bulk dopamine. To confirm this, we carried out oxidation of bulk dopamine and DA NPs containing an equivalent concentration of dopamine (Figure S2) in the presence of sodium periodate ($NaIO_4$) as per an earlier report.[36] The UV−visible spectra of oxidized products of dopamine and DA NPs, recorded at various time points, are shown in Figure S2. We observed that the dopamine, which remained inside the matrix, was not available for oxidation. On the basis of this finding, it was presumed that nanotization made our prepared DA NPs more stable against oxidative damage, which would result in minimizing the formation of oxidative

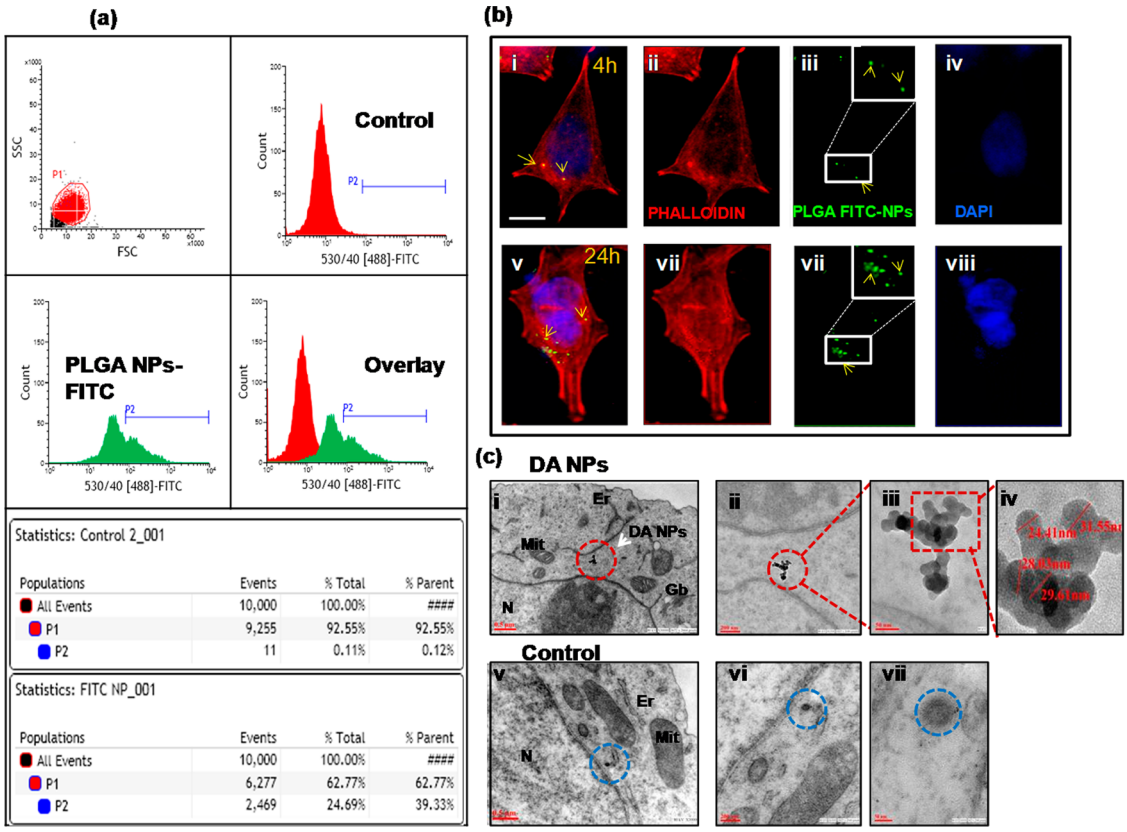


**Figure 3. Photomicrographs showing internalization of NPs by SH-SY5Y human neuroblastoma cells. SH-SY5Y cells were incubated with PLGA NPs-FITC or DA NPs suspended in culture media, for 4 or 24 h. (a) Flow cytometric assessment in the FITC channel recorded a substantial population of cells as FITC +ve after 4 h exposure to PLGA NPs-FITC. (b) Representative fluorescent photomicrographs of SH-SY5Y cells showing PLGA NPs-FITC ingress after 4 and 24 h incubation. The cells were visualized using rhodamine phalloidin (red) and DAPI (blue). The insets in iii and vii are higher magnification areas marked by white rectangles where the presence of PLGA NPs-FITC (green) was marked by arrowheads (scale bar = 20 $\mu$m). (c) TEM photographs of DA NPs-exposed (i−iv) and control (v−vii) SH-SY5Y cells. The presence of nanoparticles (red circle) in the cytoplasm of DA NPs-exposed cells was evident following 4 h incubation. Subpictures iii and iv illustrate particle morphology and size. Control cells also showed an electron-dense black spot (v, blue circle), but higher magnification (vi and vii) using a bottom-mount camera exhibited its nonspecificity (scale bar = 0.5 $\mu$m for i and v, 200 nm for ii and vi, and 50 nm for iii and vii). Mit = mitochondria, Er = endoplasmic reticulum, Gb = Golgi body, N = nucleus, DA NPs = dopamine nanoparticles.**

metabolites. Therefore, this nanoformulation was used in the rest of the experiments.

***In Vitro* Interaction of DA NPs with SH-SY5Y Dopaminergic Cells.** *DA NPs Internalized in the Dopaminergic Cells.* Cellular uptake of the prepared DA NPs using a combination of flow cytometry, fluorescent tracking, and TEM was assessed. This is important, as dopamine cycling is an integral part of its circuitry. It involves continuous dopamine trafficking from the soma of dopaminergic neurons to the axonal terminal and shuttling in and out of neuronal storage vesicles to the synaptic vicinity.[37] Dopamine synthesized or released from somato-axonal or dendritic terminals when in surplus is taken up and shipped to storage vesicles through specific uptake carriers, *viz.*, dopamine transporter (DAT) and vesicular monoamine transporter 2 (VMAT2), respectively.[38] These transporters are expressed throughout the neuronal soma and axons.[39−41] This stored dopamine is released when required and may activate either local or more distant receptors through volume transmission. This is a natural phenomenon with great significance, which prevents dopamine wastage by metabolic degradation and also is a means to impart protection from an excess of its toxic metabolites.

We then ascertained whether DA NPs undergo cellular accumulation, which we thought significant, as it could be used to replenish vesicular dopamine stores. We studied neuronal uptake/internalization of NPs using fluorescent PLGA NPs-FITC in dopaminergic SH-SY5Y cells, a model of dopaminergic neurons. This cell line expressed dopaminergic markers for dopamine synthesis (TH), transport (DAT and VMAT2), and transmission (dopamine receptors) (Figure S3). Cultures of SH-SY5Y cells were incubated with PLGA NPs-FITC for 4 h to study internalization of NPs in neuronal cells using a flow cytometer (Figure 3a). The fluorescence intensity in the cells exposed to PLGA NPs-FITC was assessed in the FITC channel. Prior to recording, these cells were washed with PBS to eliminate free NPs. We recorded the high mean fluorescence intensity (MFI) in the cells exposed to fluorescent NPs in comparison to control cells (Figure 3a). However,

on the basis of flow cytometric analysis, we were not able to differentiate whether this fluorescence is a result of interaction of PLGA NPs-FITC with the cell membrane or actual uptake of FITC-tagged NPs by the cells has taken place. Therefore, we next exposed SH-SY5Y cells to PLGA NPs-FITC for 4 and 24 h and investigated their intracellular internalization by fluorescence microscopy (Figure 3b). The location of NPs was visualized by staining the cells with rhodamine phalloidin and nuclear dye DAPI. We observed substantial incorporation of FITC-tagged PLGA NPs into SH-SY5Y cells following 4 and 24 h incubation (Figure 3b). The majority of the FITC-tagged NPs were found to be localized within the cytoplasm of SH-SY5Y cells. The uptake was found to be time dependent, as the particle internalization was greater following 24 h ($7 \pm 4$) exposure when compared to 4 h ($4 \pm 1$) by counting nanoaggregates. A time- and concentration-dependent uptake of PLGA NPs was also reported earlier.[42] This was in agreement with our previous study, where curcumin-loaded PLGA NPs were found to be internalized by neurons, astrocytes, and neural stem cells.[23] Internalization of polyethylenimine- and PLGA-based NPs by adult neuronal cells was also demonstrated in previous studies.[43,44] Clathrin-mediated endocytosis was reported to be involved in the process of internalization of PLGA NPs.[26]

We observed similar findings in TEM analysis (Figure 3c). DA NPs-exposed cells, scanned using a side-mount camera, showed the presence of electron-dense nanoparticles in the cytoplasm (Figure 3c; i arrow marked red circle). We confirmed their identity by morphology and size assessment using a bottom-mount CCD camera used for materials (Figure 3c; ii−iv). SH-SY5Y cells that were not exposed to DA NPs were also assessed in parallel to serve as a negative control (Figure 3c; v−vii). An electron-dense dark spot was also visible there (Figure 3c; v, blue circle), but high-magnification visualization through a bottom-mount CCD camera showed their nonspecificity (Figure 3c; vi and vii). Our earlier studies have also reported the presence of curcumin- and nicotine-encapsulated PLGA NPs in the brain, following systemic administration.[23,25]

*DA NPs Are Less Cytotoxic than Bulk Dopamine.* The above findings suggested that DA NPs interacted with cells and internalized in the cytoplasm. We hypothesized that the internalization of NPs would influence cellular functions and viability. Therefore, we next evaluated the safety of DA NPs by studying the effects of different concentrations of DA NPs on viability, mitochondrial activity, morphology, and reactive oxygen species (ROS)-mediated changes in SH-SY5Y cells and compared it with bulk dopamine. This was a prerequisite, as our formulation incorporated dopamine, which if left unguarded, readily forms ROS. In cells, dopamine is stable only inside the synaptic vesicles maintained at low pH.

The excess cytosolic dopamine existing outside the synaptic vesicles is prone to metabolism *via* monoamine oxidase (MAO) or by autoxidation.[45] During the oxidation of dopamine by MAO, several oxidative molecules including $H_2O_2$, and 3,4-dihydroxyphenylacetic acid (DOPAC) are generated.[46] Conversely, nonenzymatic and spontaneous autoxidation of dopamine produces $O_2^{\bullet}$ and reactive quinones.[47] This was important, considering our aim to deliver dopamine into the PD brain, where with the demise of dopaminergic neurons the dopamine transport and vesicular storage were also disrupted.

We exposed SH-SY5Y cells to bulk dopamine (2−300 $\mu$g/mL) and a corresponding concentration of DA NPs for 24 (Figure S4a) and/or 48 h (Figure 4). Exposure to bulk dopamine for 48 h resulted in significant cell death at 100 and 300 $\mu$g/mL concentrations, as assessed by the trypan blue assay (Figure 4a). In contrast, DA NPs were not found to cause significant cell death at any test concentration. Similarly, SH-SY5Y cells exposed to PLGA NPs, which were void of dopamine, did not exhibit any significant loss of cell viability at any test concentration (data not shown). These findings correlate well with the earlier reports where polymer-encapsulated L-DOPA formulations were found to be less toxic than L-DOPA when exposured to NT3 or PC12 cells, respectively.[48,49]

We also assessed the changes in mitochondrial activity through the 3-(4,5-dimethylthiazol-2-yl)-2,5-diphenyltetrazolium bromide (MTT) reduction assay. Both bulk dopamine and DA NPs did not cause significant alteration in MTT reduction at lower concentrations (2−50 $\mu$g/mL) (Figure 4b). Exposure to bulk dopamine at higher concentrations (100 and 300 $\mu$g/mL) for 48 h resulted in a significant decrease ($p < 0.05$ and $p < 0.01$) in mitochondrial activity (Figure 4b). This observation was in line with earlier reports, where dopamine at 100 $\mu$g/mL or above caused significant impairment in mitochondrial activity, accompanied by cell death.[46,50] In contrast, DA NPs, corresponding to dopamine concentrations of 100 and 300 $\mu$g/mL, caused increased ($p < 0.05$, $p < 0.01$) MTT reduction, suggesting enhanced mitochondrial function (Figure 4b). A similar trend of an increase in PC12 cell proliferation on exposure to dopamine was reported earlier,[51] which was explained on the basis of dopamine-D1 receptor-mediated protection. Similarly, dopamine was also reported to show an antioxidant property,[52] which could be one of the reasons related to the proliferative effect of DA NPs in the present experiment. We anticipated that both encapsulation of dopamine, which made it safe from liberal oxidation, and controlled release of dopamine from DA NPs together confined dopamine concentration well below the toxic threshold, which in turn masked its toxic effects and favored proliferation. Our results are consistent with earlier studies reporting enhanced proliferation of

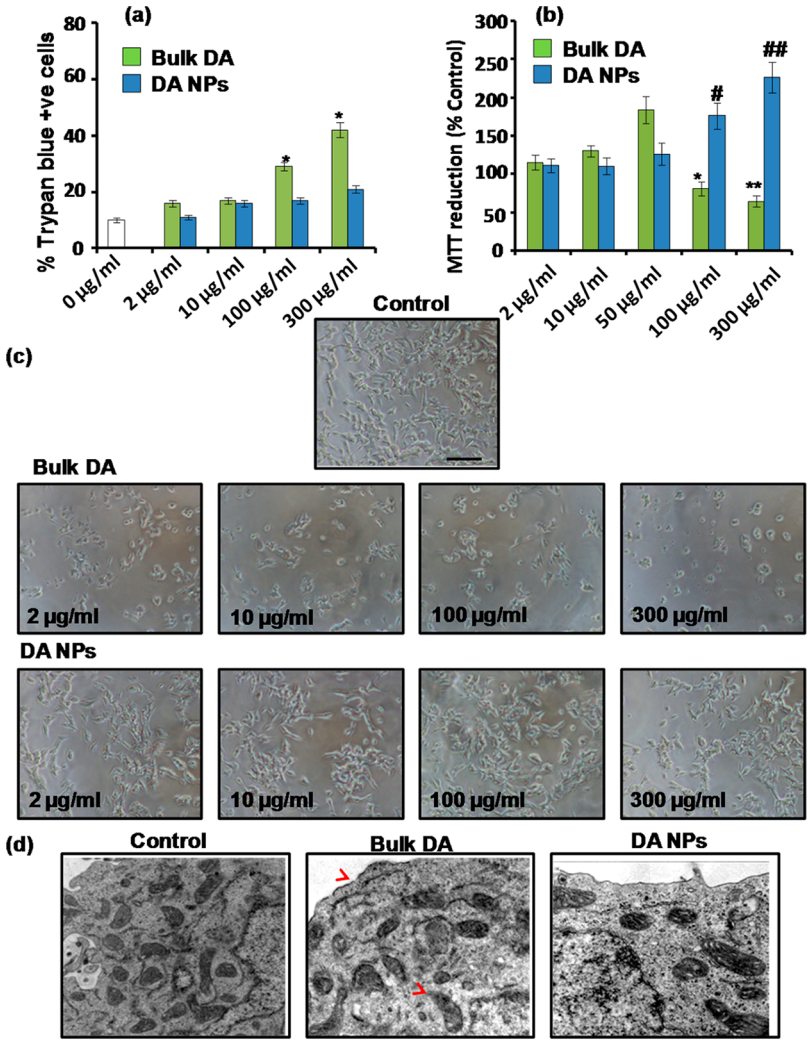


**Figure 4. Effect of bulk dopamine (2 to 300 $\mu$g) and equivalent concentrations of DA NPs on SH-SY5Y cells. (a) Trypan blue exclusion assay: Cells were exposed to various concentrations of bulk dopamine and DA NPs for 48 h, and loss of cell viability was measured. (b) Spectrophotometric measurement of changes in mitochondrial activity as MTT reduction. Data are mean ± SE of $n = 3$ in triplicate. $^{*,\#}$Significantly different from respective control, $^{*,\#}p < 0.05$, $^{**,\#\#}p < 0.01$. (c) Representative phase contrast photomicrographs showing concentration-dependent changes in morphology of cells following 48 h exposure to bulk dopamine and DA NPs. Scale bar = 100 $\mu$m. (d) TEM photomicrographs representing ultrastructural changes in cells after 48 h exposure to 100 $\mu$g/mL bulk dopamine and DA NPs. Bulk DA = bulk dopamine, DA NPs = dopamine nanoparticles.**

precursor population in the subventricular zone by dopamine.[53] Dopamine is also reported to stimulate epidermal growth factor (EGF) release and activation of EGF receptors, while dopamine depletion resulted in impaired cell growth.[54,55]

We reanalyzed our findings on the basis of morphological changes and formazan crystal appearance. We recorded abnormal cell morphology, with smaller and round cells at different concentrations of bulk dopamine, which caused a significant decrease in MTT reduction (Figure 4c). However, DA NPs did not produce morphological alterations at the same concentrations studied. This again suggested that slow and constant release of dopamine from NPs produced significantly less morphological deterioration. Further, the formazan crystals produced by bulk dopamine had lost their normal star-like appearance, and crystals appeared blunt and small (Figure S4b). On the basis of these results, we deduced that on application of higher bulk dopamine concentration, the cells got stressed, possibly due to the generation of ROS. These results were in accordance with an earlier study, where dopamine and L-DOPA caused significant morphological alterations in neuronal cells.[51]

The differential effect of bulk dopamine and DA NPs was also evident in ultrastructural changes in SH-SY5Y cells (Figure 4d). Control SH-SY5Y cells showed a substantial number of normal mitochondria with preserved crista architecture (Figure 4d). The bulk dopamine-treated cells, however, showed a discontinuous cell membrane. The mitochondria also exhibited membrane damage and significant crista fracture (Figure 4d). Cells exposed to DA NPs, however, did not exhibit any such abnormality. In DA NPs-treated cells, the cell membrane was intact and the mitochondrial membrane was also continuous with

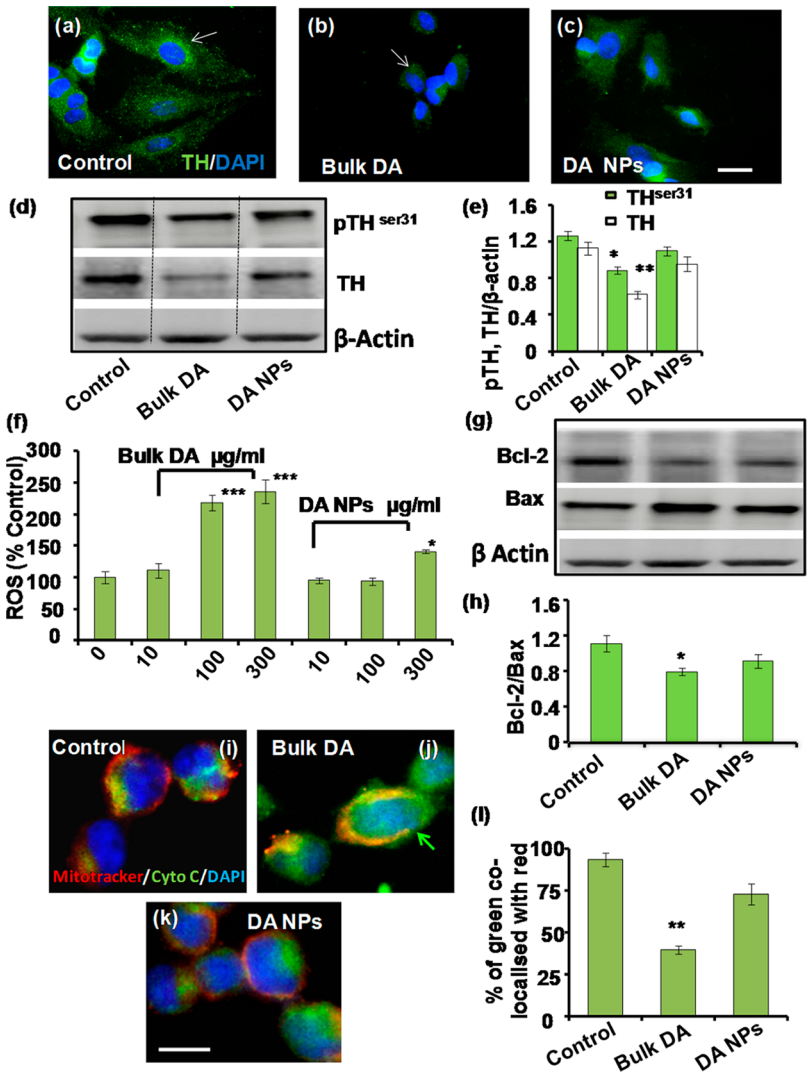


**Figure 5. Effect of exposure to bulk dopamine (100 $\mu$g/mL, 48 h) and equivalent concentration of DA NPs on tyrosine hydroxylase (TH) expression and its relation to ROS-mediated mitochondrial impairment in SH-SY5Y cells. Representative photomicrographs (a−c) show changes in immunolabeling for TH (arrow). Bulk dopamine-exposed SH-SY5Y cells (b) showed substantial loss of TH expression when compared to control (a) and DA NPs-exposed (c) cells. (d) Blots of TH expression and activation (phosphorylation at ser31) and (e) its quantification. Significant loss of TH and its activity was evident on bulk dopamine exposure. (f) Concentration-dependent increase in ROS generation higher in bulk dopamine-treated cells than in DA NPs-treated group when compared to untreated cells. (g) Representative immunoblots of Bcl-2/Bax expression and (h) their quantification. Significant down-regulation of Bcl-2:Bax occurred in bulk dopamine-exposed cells when compared to control. (i to k) Representative photomicrographs of control (i), bulk dopamine (j), and DA NPs (k) exposed SH-SY5Y cells colabeled with Mitotracker Deep Red and anti-cytochrome *c* (Cyto C) antibody. Increased cytosolic presence of Cyto C expression (green arrow) was evident in bulk dopamine-exposed cells when compared to control. (l) Graphical representation of % of co-localization (Manders' co-localization coefficient) of green (Cyto C) with red (mitotracker deep red). Scale bar = 50 $\mu$m. Data are mean ± SE of $n = 3$ in triplicate. *Significantly different from control, *$p < 0.05$, **$p < 0.01$, ***$p < 0.001$. Bulk DA = bulk dopamine, DA NPs = dopamine nanoparticles.**

well-preserved crista architecture. The observed morphological alterations in the mitochondria by bulk dopamine could be due to the generation of a high amount of ROS by dopamine. In contrast, in DA NPs-treated cells, dopamine was released slowly, which possibly did not produce sufficient ROS in culture to cause toxicity.

A similar trend was also emulated in our following experiment, where bulk dopamine caused a significant down-regulation of tyrosine hydroxylase (TH) expression and activity (Figure 5b,d,e). TH is an intermediate enzyme of dopamine biosynthesis and reflects dopaminergic neuron function.[56] An equivalent concentration of DA NPs did not cause significant TH alterations (Figure 5c,d,e) when compared to control (Figure 5a,d,e). Significant ROS generation (Figure 5f), observed in the presence of higher concentrations (100 and 300 $\mu$g/mL) of bulk dopamine, can be linked to the above observations. Earlier studies have reported enhanced ROS generation by dopamine or its oxidation products.[57,58] Further, enhanced ROS levels were also reported to inhibit TH.[59] Therefore, significantly decreased TH levels

observed in our study by bulk dopamine treatment could be due to enhanced ROS generation by dopamine itself. In contrast, DA NPs produced significant ROS only at 300 $\mu$g/mL, when compared to control (Figure 5f). Going further downstream, we examined a panel of anti- and pro-apoptotic proteins related to mitochondrial function and susceptible to change by oxidative metabolites of dopamine (Figure 5g–l). Mitochondrial dysfunction was implicated in apoptosis, where localization of the anti-apoptotic Bcl-2 was reported to be decreased at the outer mitochondrial membrane.[60] Proper expression and location of Bcl-2 is important, as it inhibits the efflux of cytochrome *c*, which is a link between mitochondrial events and the activation of the proteolytic caspase cascade.[61] It also keeps check on pro-apoptotic protein Bax. Bax is known to form channels in the mitochondrial membrane through oligomerization and thereby facilitates the cytosolic release of cytochrome *c*. Cytosolic cytochrome *c* in turn promotes associated caspases and apoptosis.[62] Therefore, the ratio of Bcl-2 to Bax is important for normal mitochondrial function and cellular viability. We examined the levels of Bax and Bcl-2 through Western blot (Figure 5g,h). We observed a significant decrease in the protein ratio of Bcl-2 to Bax in bulk dopamine-exposed SH-SY5Y cells, when compared to control, 48 h postexposure. However, no significant decrease in Bcl-2:Bax was observed in the DA NPs-treated group. Earlier, dopamine itself reportedly induced apoptosis through alteration of the Bax/Bcl-2 ratio.[63,64] Therefore, NP-mediated delivery of dopamine significantly prohibited apoptosis by preventing alterations in the Bcl-2:Bax ratio in cells.

As the above changes may lead to mitochondrial permeability transition, we further analyzed this by studying localization of cytochrome *c* on exposure to bulk dopamine and DA NPs. Cytochrome *c* is retained in intact mitochondria between intermembrane and intracristal spaces.[61] In the event of any disruption in mitochondrial permeability, it leaks into the cytosol.[65] Double labeling of cells with Mitotracker Deep Red and cytochrome *c* antibody was performed to study mitochondrial function. Control SH-SY5Y cells depicted distinct co-localization of cytochrome *c* (green) with Mitotracker Red (Figure 5i, Mander's co-localization coefficient; $M = 0.938$). Bulk dopamine-treated cells exhibited a pronounced diffused cytosolic pattern of cytochrome *c* immunoreactivity (Figure 5j) and decreased localization in mitochondria ($M = 0.339$). Interestingly, DA NP exposure did not cause significant cytosolic localization of cytochrome *c* (Figure 5k, $M = 0.73$). A related finding earlier reported disruption in mitochondrial membrane potential by dopamine and its precursor L-DOPA,[66] which was protected in our study by the application of DA NPs.

***In Vivo* Study.** The therapeutic potential of DA NPs administration was next evaluated *in vivo* by studying plasma pharmacokinetics of DA NPs *vs* bulk dopamine, delivery of DA NPs across the BBB, and their restorative potential in a 6-OHDA-induced rat model of PD. Further, as our preparation involves dopamine, which is prone to oxidative metabolism, we studied the level of oxidative stress-mediated effects caused by DA NP administration and its influence on the endogenous dopamine system. Since DA NPs were administered intravenously, we further evaluated the effect of their infusion on the cardio vascular system (CVS).

*Enhanced Plasma Retention of DA NPs in Comparison to Bulk Dopamine.* The plasma pharmacokinetics of dopamine following iv administration of bulk dopamine and DA NPs was studied (S5). In the DA NP formulation, the polar nature of dopamine was masked. Its systemic clearance was also reduced, and in turn a higher delivery of dopamine into the brain can be anticipated. After intravenous administration as DA NPs, the systemic plasma clearance of dopamine was significantly reduced (from 108.17 mL/min/kg to 21.19 mL/min/kg), and the plasma half-life of dopamine was increased (from 1.22 h to 2.53 h) in comparison to the bulk dopamine administration. A considerable dopamine level (~45 ng/mL) upon DA NP treatment was recorded up to 6 h, which is greater than the basal plasma levels of dopamine in the rats (<0.5 ng/mL).[67]

Further, the benefit of the above observation was evident in our later experiment in the form of increased levels of dopamine in the rat striatum following DA NP exposure. A recent related study reported that NPs of PLGA-encapsulated antiparkinsonian drug L-DOPA significantly enhanced L-DOPA half-life, bioavailability, and efficacy when delivered to the brain through intranasal administration.[68] Similarly, dopamine delivery through intraperitoneal administration of dopamine-loaded chitosan NPs resulted in increased levels of dopamine in the striatum of the rat brain.[69]

*Successful Delivery of PLGA NPs-FITC and DA NPs to Striatum after Intravenous Injection.* DA NPs must cross the BBB in order to deliver the dopamine in the striatal region, which was required for restoring the functional deficits related to dopamine deficiency. To evaluate in-brain delivery of NPs in rats, we studied the distribution of FITC-tagged PLGA NPs and DA NPs in the striatal region 4 h and 7 days post-iv injections, respectively. Fluorescent microscopic analysis showed the presence of PLGA NPs-FITC in the striatum of control, sham, and 6-OHDA-lesioned animals (Figure 6a–c). Significant fluorescence signal was detected in detergent-soluble fractions of the homogenate of the striatum from PLGA NPs-FITC-injected animals. Detectable accumulation of FITC-tagged DA NPs in the striatal region of control, sham, and 6-OHDA-lesioned animals was observed (Figure 6e), as calculated from a standard plot of PLGA NPs-FITC (Figure 6d). Specificity of signal was confirmed by comparing with an experimental control injected with nonfluorescent PLGA NPs (data not

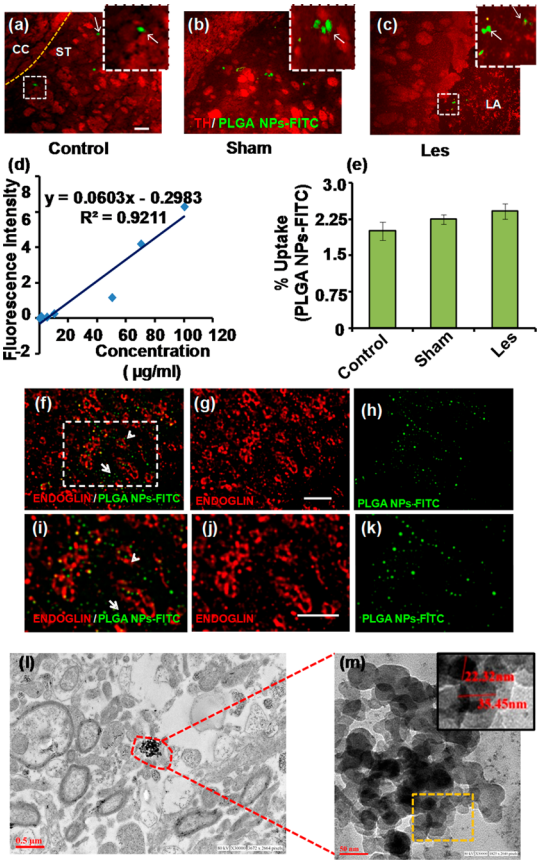


**Figure 6. (a–c) Representative fluorescent photomicrographs of rat brain striatal sections (marked by immunoexpression for TH, red) of control, sham, and 6-OHDA-lesioned (Les) animals illustrating *in vivo* uptake of iv-administered PLGA NPs-FITC, 4 h postinjection. Insets in a–c are higher magnification of area enclosed in a small rectangle showing PLGA NPs-FITC (white arrow). (d) Standard curve of PLGA NPs-FITC obtained after spiking the striatum of control animals with serially diluted NP suspensions (0.3–100 $\mu$g/mL). (e) Percent uptake of PLGA NPs-FITC in control, sham, and Les rats. (f–h) Transport of intravenously injected PLGA NPs-FITC (arrow) outside blood capillaries (arrowhead) immunomarked with anti-endoglin antibody in rat brain striatal sections. (i–k) Higher magnification of area marked with dotted lines in part f. (l) TEM photomicrograph showing the presence of DA NPs aggregating in the striatal sections of rats 7 days post-iv infusion, captured with a bottom-mounted camera used for materials. (m) Higher magnification of area marked by a red circle in part l. Inset in m illustrates higher magnification of the area marked with dotted lines showing the size of NPs in the nanoaggregate. Scale bar = 200 $\mu$m for a–c, 50 $\mu$m for f–k, 0.5 $\mu$m for l, and 50 nm for m. CC = corpus callosum, ST = striatum, LA = lesioned area. *n* = 3.**

shown). In our previous study also, we found that PLGA NPs-FITC reached the hippocampus and subventricular zone of the rat brain.[23]

The detection of fluorescence emission in the brain homogenate did not discriminate between NPs being confined within blood capillaries/microvasculature or leaving this domain to reach the brain parenchyma (neurons and glial cells). To determine the brain localization of NPs at a microscopic level, we conducted double immunofluorescence microscopic analysis 4 h after intravenous injection of PLGA NPs-FITC in the rats. The representative photomicrographs of the striatal region (Figure 6f–k) illustrate capillaries stained in red by marker antibody endoglin (Figure 6g,j), while the presence of PLGA NPs-FITC was marked by green (Figure 6h,k). We observed the presence of NPs both inside and outside labeled vessels/capillaries (Figure 6f,i).

Their extravasation to the brain parenchyma was further confirmed by labeling the striatal sections from PLGA NPs-FITC-infused rats (*n* = 3) with neuronal and glial markers $\beta$-tubulin and glial fibrillary acidic protein (GFAP), respectively. We could detect FITC signals near and inside the neuron and astrocytes, confirming their reach to these cells (Figure S7). These findings are of interest, as DA NPs internalized in astrocytes may act as a reservoir for dopamine. A recent study has suggested that striatal astrocytes may act as a storage site for dopamine precursor L-DOPA.[70]

Striatal localization of DA NPs was further verified at the ultrastructural level by TEM. We observed polymeric NP aggregates located in the striatal region (Figure 6l,m). The NPs' identity was established by studying their shape and size with the help of a camera used for material sciences. Our recent study also showed localization of curcumin-loaded PLGA NPs in the neuronal and glial cells of the hippocampus in the rat brain.[23]

*DA NP Administration Restored Functional Deficits in a 6-OHDA-Lesioned Rat Model of PD.* The biodistribution study demonstrated the delivery and presence of DA NPs in the brain striatum. Next, we focused on our ultimate goal, which was to explore the utility and efficacy of DA NPs in providing functional relief in a rat model of PD. This model exhibits key features of an impaired dopamine system, *viz.*, decrease in the striatal dopamine levels, and dopamine-D2 receptor supersensitivity. We prepared this model by unilateral stereotaxic lesioning of the rat brain nigrostriatal pathway through 6-OHDA.[71] The nigrostriatal dopaminergic system innervates the dorsal striatum. Its disruption led to severe degeneration of dopaminergic neurons. We next measured the content of dopamine and its metabolites DOPAC and homovanillic acid (HVA) in the striatum by high-performance liquid chromatography (HPLC). DOPAC and HVA were taken as indirect indices of dopamine content. 6-OHDA-lesioning caused a marked decrease in levels of striatal dopamine and its metabolites DOPAC and HVA in lesioned striatum, when compared to the sham (Figure 7a). This model further exhibited marked adaptation in striatal D2 receptors in the form of supersensitivity. We observed a significant increase in striatal $^3$H-spiperone binding in the lesioned striatum, when compared to the sham (Figure 7b). Scatchard analysis showed the increase was due to the enhanced number of binding sites (Figure 7c). Earlier, we and others have reported that in

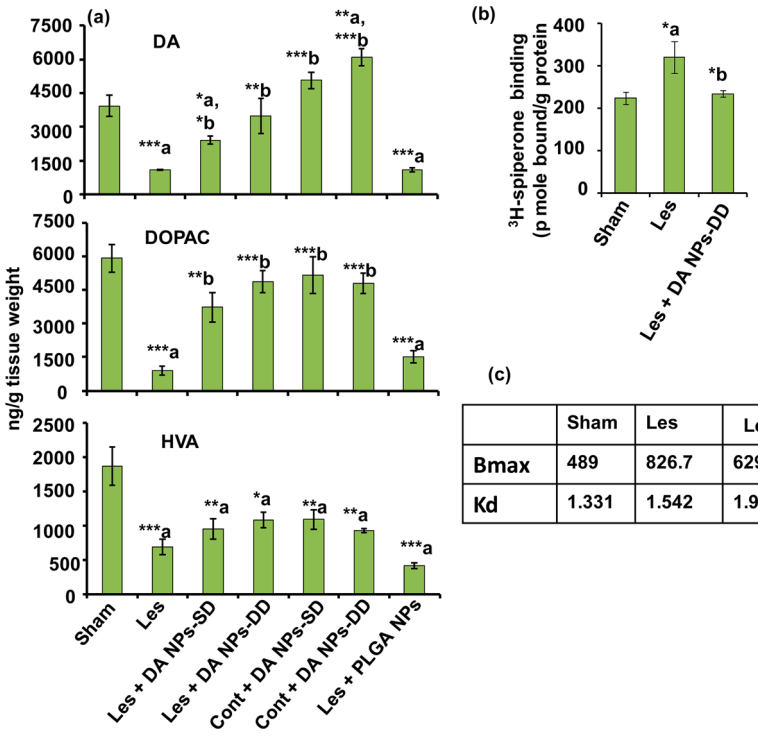


| | Sham | Les | Les + DA NPs-DD |
|---|---|---|---|
| Bmax | 489 | 826.7 | 629.4 |
| Kd | 1.331 | 1.542 | 1.936 |

**Figure 7. (a) Levels of dopamine and its metabolites (DOPAC and HVA) in the rat brain striatal region (ipsilateral in the case of all Les groups), 7 days after last iv injection of DA NPs or PLGA NPs. The test groups also include sham, Les, or control rats with single or double infusion of DA NPs. Values are expressed as ng/g wet tissue weight and represent mean ± SE of 5 rats. (b) Dopamine-D2 receptor binding in the ipsilateral striatal region of rats (sham, Les, and DA NPs-DD) 7 days after last iv administration. Values expressed as pmol bound/g protein are mean ± SE of 5 animals in each group. (c) Scatchard analysis of binding of $^3$H-spiperone (in triplicate) to rat brain striatal membrane (lesioned side) of various test groups (sham, Les, and Les + DA NPs-DD). Value of dissociation constant ($K_d$) expressed in nM and maximum number of binding sites ($B_{max}$), in pmol bound/g protein, were determined by linear regression using GraphPad Prism. *Significantly different (*$p < 0.05$, **$p < 0.01$, ***$p < 0.001$), a = compared to sham, b = compared to Les. DA NPs-SD = single infusion of DA NPs; DA NPs-DD = two infusions of DA NPs at 1-day interval.**

response to the lesion-induced decrease in the levels of dopamine in the striatum, the dopamine-D2 receptors become supersensitive.[56,72] This is so because dopamine checks the inhibitory effects of striatopallidal inhibitory GABAergic neurons by acting on striatal dopamine-D2 receptors localized on their cell bodies.[73] A comparable increase in dopamine-D2 receptors was also reported in Parkinson-related and idiopathic Parkinson's patients.[74]

Next, we studied the therapeutic effects of intravenous DA NP infusion on the restoration of dopamine levels, and striatal $^3$H spiperone binding to dopamine-D2 receptors in the rats (Figure 7a and b). For this, rats of various groups were given either a single intravenous infusion of DA NPs (DA NPs-SD) or two infusions (DA NPs-DD) at an interval of 1 day, and the assessments were made 7 days after the last injection. Lesioned animals infused with PLGA NPs were considered as particle control. Selection of the iv route was based on earlier reports describing it as the only method for effective dopamine administration due to its rapid peripheral metabolism and susceptibility to alkaline pH.

Single and double doses of DA NPs enhanced the dopamine levels significantly, when compared to lesioned. The increase in dopamine levels was more in animals receiving a double infusion of DA NPs (Figure 7a). This was anticipated considering the slow and sustained release of dopamine from NPs. Infusion of PLGA NPs that contain no dopamine showed no recovery in dopamine levels.

Next we evaluated changes in dopamine-D2 receptors to further confirm the efficacy of the DA NP formulation in providing neurorestoration. Lesioned animals when given a double infusion of DA NPs showed a significant decrease in striatal $^3$H-spiperone binding when compared to lesioned rats (Figure 7b,c). The decrease was due to the decrease in $B_{max}$ of the receptors. Our results are substantiated by an earlier study, where direct intrastriatal delivery of dopamine significantly decreased dopamine-D2 receptor supersensitivity in a 6-OHDA-induced PD model.[72] These results further supported that dopamine released in the brain *via* NPs is capable of reversing the dopamine receptor changes caused by lack of this neurotransmitter. These findings become more relevant in advanced stages of degeneration, where the released pool of dopamine could not be replenished by just dopamine precursors due to the loss of controlled dopamine transport and storage machinery, which

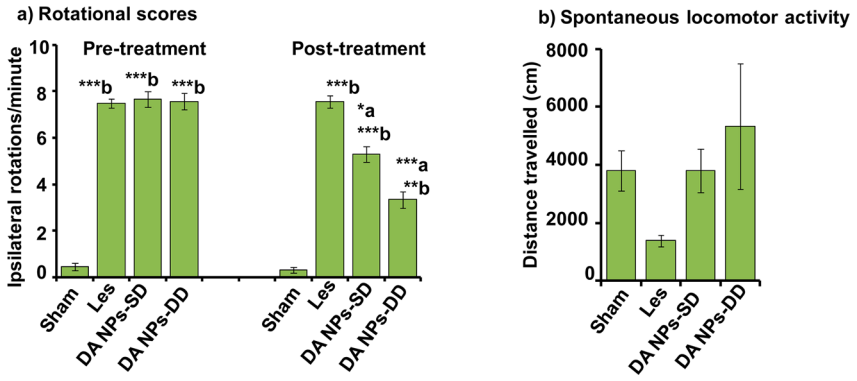


**Figure 8. (a) Rotational scores of sham, Les, and Les rats treated with a single or double dose of DA NPs. Seven days after the last NP injection, rats were challenged with D-amphetamine 5 mg/kg b.wt ip, and 30 min later full body turns ipsiversive to the lesioned side were recorded for 10 min. (b) Spontaneous locomotor activity of sham, Les, and single or twice DA NPs-infused Les rats, 7 days after iv infusion. Data are mean ± SE of 5 animals. *Significantly different (*$p < 0.05$, **$p < 0.01$, ***$p < 0.001$). a = *vs* respective pretreatment score, b = *vs* sham. DA NPs-SD = single infusion of DA NPs, DA NPs-DD = two infusions of DA NPs at 1-day interval.**

results in an imbalance between stimulation of D1 and D2 receptors, causing a loss of synergic activity of direct and indirect input pathways.[75] The L-DOPA or nano L-DOPA formulation may become ineffective in this state and can possibly aggravate symptoms, such as dyskinesia.

As any impairment in the level of dopamine and its receptors leads to alteration in motor behavior including locomotor activity, we studied the effect of DA NP administration on neurobehavioral function in parkinsonian rats. We selected amphetamine-induced rotation for this purpose. Amphetamine causes uneven release of dopamine between lesioned and unlesioned striatal lobes in rats with a unilateral 6-OHDA lesion, making it rotate in the ipsilateral direction. This is an essential quantitative index of striatal lesion severity.[56,71,76] We compared the amphetamine-induced rotational scores of sham and 6-OHDA-lesioned rats before NP infusion. The number of ipsilateral rotations was significantly increased in 6-OHDA-lesioned rats when compared to sham, depicting the efficacy of the lesion. To test the neurotherapeutic effects of DA NPs on neurobehavior, 6-OHDA-lesioned animals were then divided into three subgroups. One remained untreated, while the other two groups received a single (DA NPs-SD) or two repeated (DA NPs-DD) intravenous injections of DA NPs. We observed a significant decrease in amphetamine-induced rotations 7 days after DA NP injections when compared to 6-OHDA-lesioned rats or to their respective pretreatment scores (Figure 8a). However, the decrease in rotational scores was more pronounced in DA NPs-DD-treated rats compared to a single injection. The attenuating effect of DA NPs on rotational behavior indicated its potential antiparkinsonian activity. Next, we studied the effects of single and double infusion of DA NPs on locomotor activity in 6-OHDA-lesioned rats. 6-OHDA administration caused a decrease in locomotor activity, which was restored to sham level in DA NPs-administered rats (Figure 8b). Our results are substantiated by an earlier study, where delivery of dopamine precursor L-DOPA NPs significantly induced motor function recovery in the 6-OHDA-induced rat model of PD[68] or led to behavioral endurance in dyskinetic rats. Similarly, NP-mediated controlled delivery of L-DOPA methyl ester significantly prevented L-DOPA-induced dyskinesia in rats.[77] Overall, these results suggest that DA NPs were able to recover motor deficits in a parkinsonian rat model.

*No Adverse Effects of DA NP Administration on the Dopaminergic System of PD Rats.* To rule out any additional disturbance in dopamine circuitry of lesioned areas as a consequence of DA NP administration, we next evaluated the effect of DA NP administration on key parameters of dopamine synthesis and uptake. This was important, as our approach involved sustained release of dopamine into the brain. Surplus dopamine in the synaptic cleft or around it is prone to oxidation and can produce toxic dopamine quinone, aminochrome, and quinoprotein adducts together with numerous free radicals.[46,47] We measured the expression of TH, DAT, and quinoprotein adducts. TH is a rate-limiting enzyme for dopamine synthesis, while DAT manages dopamine levels in the brain through presynaptic uptake and transporting it to vesicles, where it is taken inside through vesicular monoamine transporter, when in excess. Covalently linked quinoprotein adducts are reaction products of dopa quinones and cellular nucleophiles such as the cysteinyl residue of glutathione, TH, and several mitochondrial proteins.[78] We observed a significant decrease in TH and DAT expression in the striatum of 6-OHDA-lesioned rats when compared to the sham (Figure 9a and b). We found no further loss of TH and DAT expression in the lesioned areas of DA NPs-administered rats when compared to 6-OHDA-lesioned rats (Figure 9a and b). These results suggested that dopamine released by DA NPs in slow and continuous

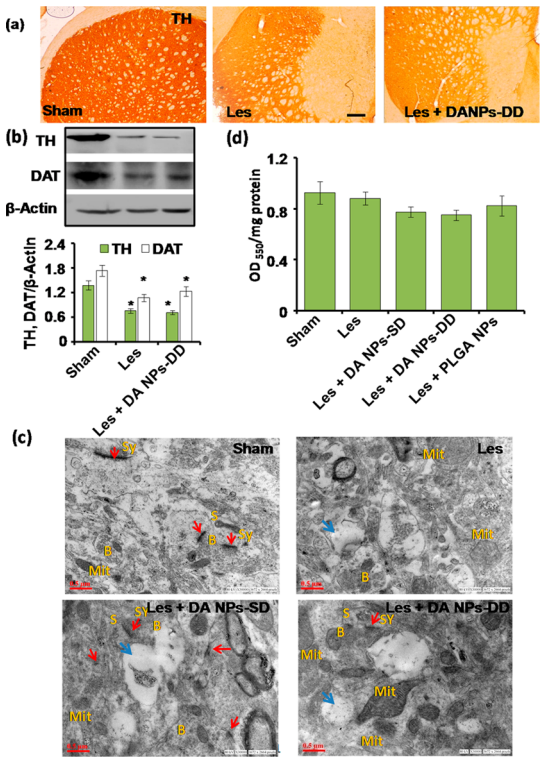


**Figure 9. (a) Representative photomicrographs showing TH-immunolabeled striatal (ST) sections (ipsilateral) of sham, Les, and twice DA NPs-infused Les rats. Les rats as such and after DA NP administration exhibited comparable loss of TH expression. (b) Western blot and densitometry of TH and DAT expression in the ipsilateral striatal region of Les and DA NPs-infused Les rats showing significant loss in TH and DAT expression when compared to the sham. (c) TEM photomicrographs showing striatal (ipsilateral) ultrastructure of the sham, Les, and rats who received a single or double infusion of DA NPs after lesioning. The sham striatum showed a number of clearly marked synapses, healthy mitochondria, and intact axonal boutans. In contrast the striatum of rats of all other groups showed a loss in synapses, swelled mitochondria, and degenerating boutans. (d) Quinoprotein estimates (expressed as $OD_{550}$/mg protein) of the striatum of sham, Les, and DA NPs/PLGA NPs-infused Les rats showed no significant difference. *Significantly differ from sham, *$p < 0.05$. Scale bar = 200 $\mu$m for a and 0.5 $\mu$m for c. Sy = synapse, B = boutan, Mit = mitochondria, S = dendritic spine.**

manner caused no deleterious effect on the dopaminergic system in the striatum. These findings were further confirmed at the ultrastructural level. Ultrastructural changes, if any, caused by DA NPs were studied by TEM analysis. In the striatum of sham rats healthy unmyelinated neurons with several normal synaptic contacts were visualized (Figure 9c). Mitochondria had a double membrane with clear cristae in control rats. In 6-OHDA-lesioned PD model rats, the mitochondria were evidently swelled and the cristae were lessened, distorted, or even absent (Figure 9c). Many degenerating axons with few diffused synaptic contacts were visible in the striatum of 6-OHDA-lesioned rats. Disintegration of synaptic contacts was also reported earlier in the *post-mortem* parkinsonian brain[79] and in the 6-OHDA-lesioned animal model.[80] DA NPs-treated animals also showed comparable peculiarities, as observed in lesioned rats (Figure 9c). These results suggest that administration of DA NPs did not cause any additional mitochondrial damage or ultrastructural changes in parkinsonian rats. Similarly, we observed that neither a single nor a double dose of DA NPs produced significant quinone adducts in the striatum when compared to lesioned and sham levels (Figure 9d).

We also observed that DA NPs after systemic administration reached the substantia nigra (Figure 10a), a region implicated in the pathogenesis of PD. We found a substantially increased number of FITC-tagged NPs in the substantia nigra of 6-OHDA-lesioned rats as compared to the sham (Figure 10b). Similar to the results of the striatum, we found DA NPs did not cause any additional change in the expression of TH and DAT in the substantia nigra of parkinsonian rats (Figure 10c). Further, ultrastructural damage was also evident in the nigral region of 6-OHDA-lesioned rats, when compared to the sham, where a number of degenerating neuronal soma were visible (Figure 10d). Mitochondria also showed significant crista fracture and membrane disorganization in the substantia nigra of 6-OHDA-lesioned rats. Similar manifestations were also observed in lesioned rats exposed to DA NPs. We observed no additional visible damage in the lesioned nigra in DA NPs-exposed animals (Figure 10d). Similarly, no significant formation of quinone adducts was found in the substantia nigra, on administration of a single or double infusion of DA NPs, when compared to sham or Lesioned rats (Figure 10e).

*DA NPs Exert No Toxicity in Nontargeted Brain Regions and Organs.* We observed that besides the striatum and nigra, intravenously administered FITC-tagged NPs were also distributed in nontargeted brain parts such as the frontal cortex (FC), hippocampus (HP), and cerebellum (CERE) 4 h post-intravenous administration (Figure S8a and b). Dopamine released in these areas from DA NPs may undergo autoxidation and thereby can induce side effects such as free radical damage. To analyze this, we further measured quinoprotein adducts in these brain parts of DA NPs-administered rats, 7 days after two intravenous injections. Quinoprotein adducts have been shown to have a strong correlation with dopamine-induced toxicity.[78] No significant difference in quinoprotein adducts of these areas was observed on comparing with respective regions of sham or 6-OHDA-lesioned rats (Figure S8c).

We could also locate many FITC-tagged NPs in the kidney, liver, and spleen of animals 4 h following intravenous administration (Figure S9a–c and j). This confirmed that a detectable portion of iv-injected NPs reached these areas. We further undertook a histopathological study of these organs following DA NP administration. When compared to the control (Figure S9d–f), we observed no detectable pathology in the liver or spleen; however the kidney of these

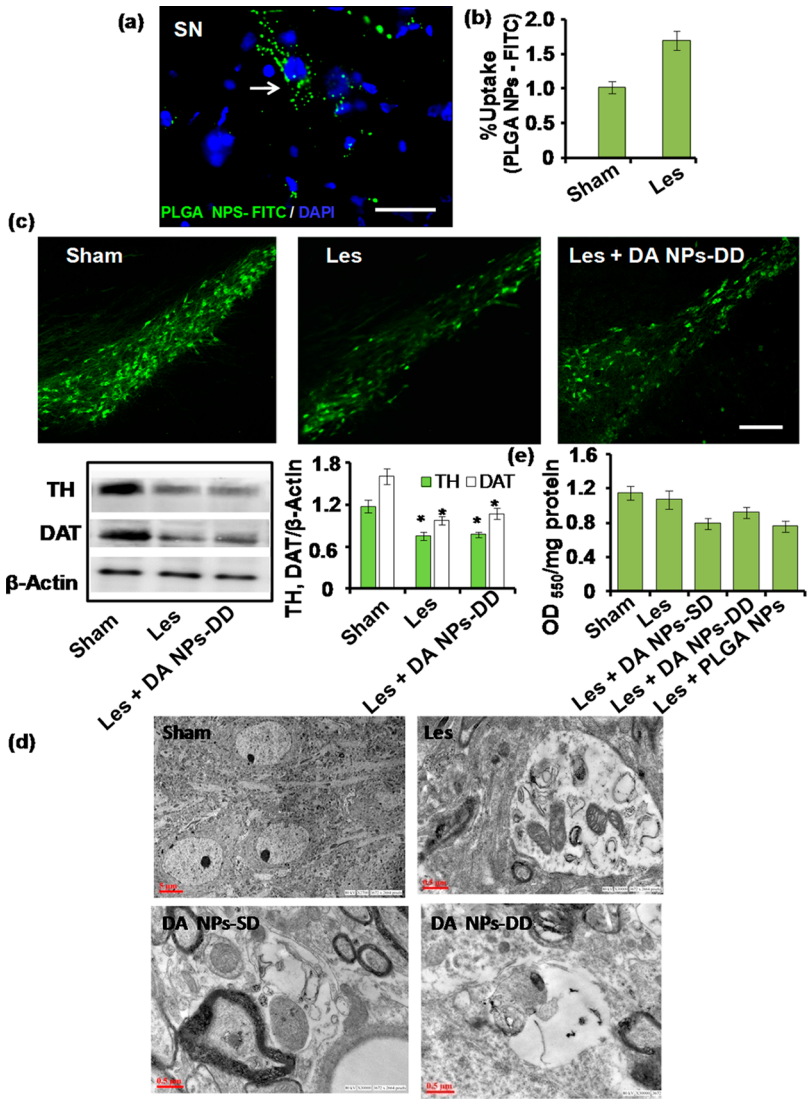


**Figure 10. (a) Representative photomicrograph of rat brain nigral (SN) sections illustrating substantial *in vivo* uptake of iv-administered PLGA NPs-FITC, 4 h postinjection. Nuclei were labeled in blue with DAPI. (b) Percent uptake of PLGA NPs-FITC quantified following 4 h infusion in the nigral region (ipsilateral) of sham and Les rats. (c) Photomicrographs showing TH-immunolabeled nigral sections and Western blot/densitometric quantification of nigral TH and DAT immunoreactivity of sham, Les, and twice DA NPs-infused Les rats. Les rats as such and after DA NP administration exhibited comparable loss of TH and DAT expression. (d) TEM photomicrographs showing the nigral ultra structure of sham, Les, and rats who received a single or double infusion of DA NPs after lesioning. Sham nigra show closely arranged neuronal cell bodies with well-marked nuclei. Lesioned nigra show formation of balloon cells depicting degenerating cell bodies carrying a number of entrapped mitochondria, and other cellular components at various stages of degeneration are clearly visible. Nigra of Les animals receiving a single or double infusion of DA NPs also show similar phenomena. (e) Nigral quinoprotein level (expressed as $OD_{550}$/mg protein) of sham, Les, and Les + single or double infusion of DA NPs or PLGA NPs showed no significant difference. Scale bar = 50 $\mu$m for (a) 200 $\mu$m for c, 5 and 0.5 $\mu$m for d. *Significantly different from sham, $p < 0.05$. Data are the mean ± SE of 4, $n = 3$. DA NPs-SD = single infusion of DA NPs, DA NPs-DD = two infusions of DA NPs at 1-day interval.**

animals showed dilated tubules (Figure S9g-i). A related finding by Hu *et al.*[26] had shown a transient inflammatory reaction in the brain and other organs of lactoferrin-conjugated PEG-PLGA NPs, which was reported to subside within a few hours.

*No Adverse Cardiovascular Effects of DA NPs.* The presence of excess dopamine in the peripheral system can exert cardiovascular effects. Therefore, we studied the effects of DA NP administration on systemic blood pressure (BP) and heart rate (HR) of rats and compared the effects with bulk dopamine. We found that PLGA NPs-FITC were present in the heart of sham and parkinsonian rats 4 h after iv administration (data not shown). Bulk dopamine produced significant alteration in the HR and BP in control rats (Figure 11a and b). DA NPs showed only a rise in HR without any change in BP. An equal amount of PLGA NPs did not produce any significant effect on BP and HR. These results suggested that sustained and slow release of dopamine from DA NPs was able to limit unwanted alterations in BP and HR. In addition, DA NP administration did not cause any remarkable histopathological change in the

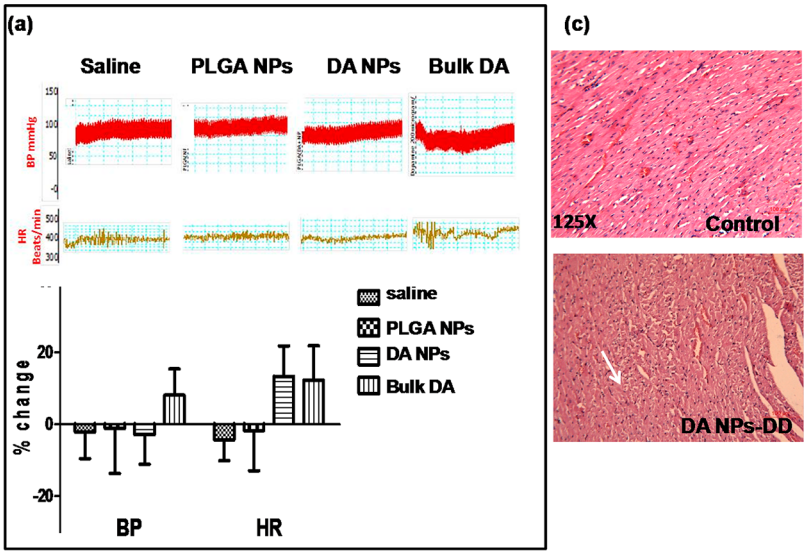


(b)

| Group | SBP | DBP | MAP | HR |
|---|---|---|---|---|
| Saline | 92.7 ± 7.5 | 61.8 ± 4.9 | 72.1 ± 5.5 | 282.9 ± 17.2 |
| PLGA NPs | 97.3 ± 8.2 | 60.6 ± 10.7 | 72.9 ± 9.3 | 290.5 ± 33.1 |
| DA NPs | 94.7 ± 7.5 | 59.9 ± 6.3 | 71.5 ± 6.0 | 335.1 ± 25.0 |
| Bulk DA 200 μg/kg | 101.5 ± 5.2 | 68.8 ± 6.5 | 79.7 ± 5.4 | 332.1 ± 28.3 |

**Figure 11. Tracings of hemodynamic parameters and its quantification in rats following iv infusion of *n*-saline, PLGA NPs, DA NPs, and bulk dopamine. (b) Effect of iv administration of *n*-saline, PLGA NPs, DA NPs, and bulk dopamine on blood pressure (BP) and heart rate (HR) of rats. (c) Representative photomicrographs showing histopathology of the heart of control and twice DA NPs (DA NPs-DD)-infused rats ($n$ = 5). SBP = systolic blood pressure, DBP = diastolic blood pressure, MAP = mean arterial pressure, bulk DA = bulk dopamine, DA NPs = dopamine nanoparticles.**

heart (Figure 11c). These results suggested that dopamine administration through NPs did not produce any abnormal cardiovascular change in rats.

## CONCLUSIONS

In the present study, we reported dopamine delivery into the brain of PD rats, through application of PLGA NPs. In conclusion, we found that DA NPs slowly and constantly released dopamine, internalized in the brain, reduced clearance of dopamine in plasma, reduced quinone adduct formation, and decreased dopamine autoxidation. These NPs significantly reversed neurobehavioral abnormalities in parkinsonian rats. Further, DA NPs did not produce additional ROS, dopaminergic neuron degeneration, and ultrastructural changes in the striatum and substantia nigra as compared to 6-OHDA-lesioned rats. These NPs did not cause alterations in the heart rate and blood pressure nor any pathological changes in the brain and peripheral organs. Overall, these results suggest that NPs delivered dopamine into the brain, reduced dopamine autoxidation-mediated toxicity, and ultimately reversed neurochemical and neurobehavioral deficits in parkinsonian rats. Our results provide evidence that DA NPs delivered dopamine into the brain, reduced dopamine associated toxicity, and recovered neurochemical and neurobehavioral alterations in PD. Thus, the DA NP formulation may provide a novel therapeutic approach for delivery of dopamine in the brain for the treatment of PD.

## MATERIALS AND METHODS

**Chemicals.** Poly(D,L-lactide-*co*-glycolide) lactide:glycolide (50:50) mol wt 30 000−60 000, dopamine hydrochloride, poly(vinyl alcohol) mol wt 30 000−70 000, 3-[4,5-dimethylthiazol-2-yl]-2,5-diphenyltetrazolium bromide (MTT), trypan blue, fluorescein isothiocyanate isomer I (FITC), *N*-Boc-ethylenediamine, paraformaldehyde, L-glutamine, dimethyl sulfoxide (DMSO), 2′,7′-dichlorodihydrofluorescin diacetate (DCFH-DA), 3,4-dihydroxyphenylacetic acid, homovanillic acid (HVA), osmium tetraoxide, glutaraldehyde, trizma base, anti-GFAP, anti-$\beta$-tubulin, and anti-TH were procured from Sigma (USA). Secondary antibodies conjugated to HRP/Alexa 488/Alexa 568, Mitotracker Deep

Red, fetal bovine serum (FBS), Dulbecco's modified Eagle's medium (DMEM): F12, phosphate-buffered saline (PBS), trypsin, antibiotic−antimycotic solution, and rhodamine phalloidin were obtained from Invitrogen (USA). Antifade mounting media Vectashield was purchased from Vector Laboratories (USA). Anti-cytochrome *c*, anti-$\beta$-actin, anti-Bax, and anti-Bcl-2 were purchased from Cell Signaling (USA). Radioligand $^3$H-spiperone was procured from Amersham (England). Anti-VMAT2 and anti-DAT were obtained from Santa Cruz Biotechnology (Santa Cruz, CA, USA). Anti-dopamine D2R and anti-endoglin antibodies were purchased from Chemicon International (USA). We procured Halt protease/phosphatase inhibitor cocktail and ECL Western blotting substrate from Thermo Fisher (USA), BioTrace NT membrane from Pall (USA), and culture ware from Nunc (Denmark). All the other chemicals were of AR grade and purchased from local companies based in India.

**Preparation of PLGA NPs and DA NPs.** DA NPs were prepared following the double emulsion solvent evaporation method with slight modifications.[81] Briefly, dopamine hydrochloride, 50 mg in 1 mL of water, was added dropwise to 100 mg of PLGA, dissolved in 5 mL of dichloromethane (DCM), followed by sonication for 5 min (30% amplitude, 50:10 pulse on:off) to generate a primary water/oil emulsion. This emulsion was dropwise added to a 1% w/v aqueous solution of PVA (20 mL) while stirring at 1500 rpm and sonicated for 5 min to get a secondary water/oil/water emulsion. Stirring was continued for 6−8 h until complete removal of organic solvent, followed by centrifugation at 10 000 rpm for 45 min at 4 °C. The pellet obtained was resuspended in water and washed twice. Finally, the nanoparticles were freeze-dried and stored at 4 °C under anhydrous conditions. Control PLGA NPs were formulated without the addition of dopamine, the rest of the protocol remaining the same.

**Preparation of FITC-Tagged PLGA NPs.** Fluoresceinylated PLGA NPs (PLGA NPs-FITC) were prepared (Figure S1) in a two-step reaction as previously reported.[23] Initially, 1 mmol of t-Boc-protected ethylenediamine was dissolved in 5 mL of DMF followed by addition of 1.1 mmol of FITC, and the mixture was stirred at room temperature in the dark for 12 h. Solvent was removed, and the residue was mixed by shaking for 1 h in a solution of trifluoroacetic acid/DCM (2 mL, 1:1, v/v). The reaction mixture was concentrated, triturated with 10 mL of DCM, and vacuum-dried to obtain fluoresceinyl-ethylenediamine. Next, fluoresceinyl-ethylenediamine was attached with PLGA (50 mg) by dissolving it in 1 mL of DMF. *N*-hydroxysuccinimide (NHS, 1.5 $\mu$g), 1-ethyl-3-(3-(dimethylamino)propyl) carbodiimide (EDAC, 2.5 $\mu$g), and triethylamine (TEA, 4 $\mu$L) were added, and the mixture was stirred for 2 h. Further, fluoresceinyl-ethylenediamine (5 $\mu$g, for 1% substitution) was added to the mixture, followed by stirring at room temperature for 6 h. A rotary evaporator was used to concentrate the mixture. The residue was partitioned between DCM and water, and the organic phase was collected and concentrated to dryness. The resulting mixture was dissolved in 2 mL of DCM and added dropwise into a solution of 1% PVA. The mixture was stirred for 3 h at room temperature and centrifuged. The pellet was washed with water and freeze-dried to obtain PLGA NPs-FITC.

**Characterization of NPs.** *Size and Zeta-Potential Measurements.* Mean particle size and zeta potential were analyzed by dynamic light scattering using a Zetasizer Nano-ZS (Malvern Instruments, Malvern, UK), employing a He−Ne laser (5 mW) operating at 633 nm wavelength. Samples were prepared by dispersing NPs in filtered water (viscosity: 0.89 cP; refractive index: 1.33) at a concentration of 0.5 mg/mL. The size and zeta potential were measured as an average of 20 and 30 runs in triplicate, respectively. The data analysis was performed in automatic mode, and the average values were calculated from the electrophoretic mobility applying the Smoluchowski approximation.[82]

*TEM Analysis.* PLGA NPs and DA NPs were suspended in water, layered over carbon-coated grids, and negatively stained prior to morphological examination. The diameter of particles was measured through Gatan digital micrograph software under a FEI transmission electron microscope (Tecnai G2 Spirit, The Netherlands) at 80 kV.

*SEM Analysis.* The polymeric NPs were characterized for their shape, surface morphology, and particle size distribution by high-resolution field emission SEM (Quanta FEG 450, FEI, The Netherlands). The polymeric sample was placed on a double-stick conducting carbon tape over an aluminum stub and coated with gold under an argon atmosphere by means of a sputter coater (SC 7620, mini sputter coater, Quorum Technology Ltd., UK). Samples were analyzed at an accelerating voltage of 5 kV and a working distance of 10 mm in a high-vacuum mode.

*Determination of Drug Loading and Entrapment Efficiency.* The amount of dopamine loading and entrapment in DA NPs were determined using a spectrophotometer. Briefly, 5 mg of DA NPs was dissolved in 1 mL of DMSO, and the absorbance of the solution was measured at 280 nm. The amount of encapsulated dopamine was calculated from the calibration curve established using standard solutions of dopamine in the same solvent. The loading and encapsulation (entrapment) efficiencies were calculated as

$$\text{Loading Efficiency}\,\% = \frac{\text{Weight of dopamine in NPs}}{\text{Weight of NPs}} \times 100$$

$$\text{Entrapment Efficiency}\,\% = \frac{\text{Weight of dopamine in NPs}}{\text{Weight of total dopamine}} \times 100$$

*In Vitro Dopamine Release Profile. In vitro* release kinetics of dopamine from DA NPs was evaluated by the dialysis method as described earlier.[23] In brief, DA NPs (10 mg) dispersed in 1 mL of PBS (pH 7.4) were transferred to a dialysis bag (molecular weight cut-off: 12 kDa) and allowed to dialyze against 10 mL of PBS with constant stirring at 100 rpm in an incubator shaker maintained at 37 °C. Aliquots (1 mL) were withdrawn at predetermined time intervals, and the container was replenished with the same amount of fresh PBS. Absorbance of the samples was measured at 280 nm. The amount of the released dopamine was calculated using a standard curve of dopamine in PBS.

*Stability Studies.* The stability of DA NPs and PLGA NPs-FITC was assessed as per earlier reports.[33−35] In brief, the nanoparticles (0.5 mg/mL) were suspended in cell culture media. The samples were incubated at 37 °C, and the hydrodynamic diameters were recorded at 1 h intervals up to 24 h using DLS as discussed above.

***In Vitro* Studies.** *SH-SY5Y Cell Culture and Characterization.* We used undifferentiated SH-SY5Y cells (ATCC) in the current study to compare the effects of bulk dopamine and DA NPs, as they are reportedly a more sensitive indicator of oxidative stress-mediated effects as compared to differentiated cells. Both undifferentiated and retinoic acid-differentiated SH-SY5Y cells are used to model neurons. However, it is reported that differentiation makes these cells less prone to oxidative stress-related changes and to dopamine neurotoxins.[83]

SH-SY5Y cells were maintained in DMEM: F12 supplemented with 10% FBS, penicillin/streptomycin (100 U/mL; 100 $\mu$g/mL), and 2 mM L-glutamine in an incubator at 37 °C with 5% $CO_2$ and 99% humidity. Cells were confirmed for the expression of marker proteins (TH, DAT, VMAT2, and dopamine-D2 receptors) using specific antibodies by immunocytochemistry prior to experiments (Figure S3).

*Cellular Internalization of NPs.* Cellular uptake of NPs was determined using flow cytometry, fluorescent microscopy, and TEM as described earlier.[23] For flow cytometry and fluorescent microscopy we used PLGA NPs-FITC, which had comparable properties to those of DA NPs. In brief, SH-SY5Y cells were seeded onto a six-well culture plate or slide flask at a density of $4 \times 10^5$ cells per well/flask. Cells were incubated 24 h later with either PLGA NPs-FITC (10 $\mu$g/mL), DA NPs, or unlabeled PLGA NPs (10 $\mu$g/mL) suspended in cDMEM: F12 media for different time intervals (4 and 24 h) in a humidified $CO_2$ incubator at 37 °C. The unlabeled PLGA NPs were used as a control.

Flow cytometry was carried out to assess the cellular uptake of PLGA NPs-FITC as per an earlier published method.[23] After exposure, the cells were washed twice with PBS to remove unbound NPs followed by trypsinization and resuspension in 500 $\mu$L of PBS. Flow cytometric analysis was carried out in the FITC channel employing an Argon 488 laser. Results are expressed in terms of mean fluorescence intensity of FITC.

For fluorescent microscopy, the cells following incubation with PLGA NPs-FITC were washed with PBS and fixed in 4% paraformaldehyde for 30 min at room temperature. The fixed cells were washed with PBS and incubated in 0.1 M glycine for 5 min. Cells were permeabilized by brief exposure (1 min) to 0.1% Triton X-100. Subsequently, the cells were incubated with rhodamine−phalloidin solution (1:3000, Invitrogen) for 30 min. The fluorescent labeled cells were washed with PBS and mounted using Vectashield aqueous mounting media (USA). Imaging was done in FITC, TRITC, and DAPI channels using a Nikon Eclipse Ti−S inverted fluorescent microscope equipped with a Nikon Digital Sight Ds-Ri1 CCD camera and NIS Elements BR 4.0 imaging software (Nikon, Japan).

TEM was performed to confirm the presence of DA NPs at ultrastructural levels in NPs-exposed cells. For this, SH-SY5Y cultures were incubated with DA NPs (10 $\mu$g/mL) suspended in cDMEM: F12 media in a humidified $CO_2$ incubator at 37 °C. After 24 h, the cells were trypsinized, washed with PBS, and processed for TEM analysis as described later.

*In Vitro Effects of Bulk Dopamine vs DA NPs Treatment.* In order to study and compare the effect of bulk dopamine and DA NPs at the cellular level, SH-SY5Y cells were plated 24 h prior to the treatment and exposed to different concentrations of bulk dopamine or DA NPs as per the experimental setup. The group without any treatment served as the control. For the trypan blue exclusion assay, the MTT assay, and morphological assessment, SH-SY5Y cells were seeded into 96-well culture plates at a density of $1 \times 10^4$ cells/well and exposed to bulk dopamine (2−300 $\mu$g/mL) or DA NPs carrying an equivalent concentration of dopamine for 24 or 48 h. ROS was estimated in the 96-well plate at a density of $1 \times 10^4$ cells/well after 48 h exposure to 10−300 $\mu$g/mL bulk dopamine or DA NPs. Significant cytotoxic effects were initiated at 100 $\mu$g/mL bulk dopamine or above; hence we used a 100 $\mu$g/mL concentration of bulk dopamine and equivalent DA NPs in our further experiments.

For TEM, Western blot, and immunocytochemistry, cells were plated onto six-well culture plates or chamber slides at a density of $6 \times 10^5$ cells/well and were exposed to 100 $\mu$g/mL bulk dopamine or equivalent DA NPs for 48 h. After treatment, the cells were analyzed for morphological and biochemical changes. All the experiments were carried out in triplicate.

*Trypan Blue Exclusion Assay.* Cell viability was evaluated by trypan blue exclusion as in our earlier study.[84] For this, SH-SY5Y cells were exposed to bulk dopamine or DA NPs as discussed above. After treatment, cells were gently trypsinized and washed with DMEM: F12 containing 10% FBS. Cells were resuspended in sterile PBS. Trypan blue solution (0.4%) was added to each sample, followed by loading onto a Neubauer chamber. An unbiased microscopic counting was carried out by a person unaware of group identity. A total of 200 cells per field were counted. Cells stained blue were marked as dead, and unstained cells were considered as live. The percent of trypan blue +ve cells among the total number of counted cells was calculated. Data are presented as percent of trypan blue +ve cells per group.

*MTT Reduction Assay.* In order to analyze the effect of bulk dopamine and DA NPs on mitochondrial integrity, the MTT assay was carried out as discussed earlier.[85] In this, formazan crystals formed by the cleavage of MTT tetrazolium salt, by mitochondrial dehydrogenases of live cells, were estimated. In brief, cells were plated in a 96-well plate. Twenty-four hours after plating, cells were exposed to bulk dopamine or equivalent DA NPs for 24 or 48 h as discussed above. After completion of treatment, 10 $\mu$L of MTT (5 mg/mL) was added to each well, and cells were incubated under 5% $CO_2$ for 4 h at 37 °C. The resulting formazan crystals formed were solubilized in DMSO (100 $\mu$L/well). Absorbance was read after 10 min at 570 nm using a Multiwell microplate reader (Synergy HT, Bio-Tek, USA). The results were calculated as percent of unexposed control.

*Morphological Assessment.* Cultured SH-SY5Y cells following treatment of bulk dopamine or DA NPs, as discussed above, were assessed for changes in morphology. A person unaware of experimental setup evaluated 10 microscopic fields of each experimental group ($n$ = 3 in duplicate) using a phase contrast microscope (Nikon, Japan). A representative photomicrograph is included in the results.

*Determination of Cellular ROS Content.* In order to assess the effect of bulk dopamine or DA NP exposure on the cellular ROS level, the redox-sensitive dye dichlorodihydrofluorescein diacetate was used as discussed earlier.[84] On oxidation by cellular ROS, nonfluorescent DCFH-DA turns to fluorescent 2′,7′-dichlorofluorescein. In brief, SH-SY5Y cells 24 h after plating onto a 96-well plate were exposed to bulk dopamine and DA NPs as discussed above. After treatment, DCFH-DA (20 $\mu$M) was added to each well, and the plate incubated for 30 min at 37 °C in the dark. Fluorescence produced by DCFH-DA was measured in a multiwell microplate reader at an excitation wavelength of 485 nm and emission wavelength of 528 nm. The results were expressed as percentage with respect to unexposed control.

*Immunocytochemistry.* SH-SY5Y cultures ($n$ = 3) following treatment were fixed in 4% paraformaldehyde at room temperature for half an hour followed by three washes with PBS. These cells were analyzed for expression of various proteins using specific anti-TH (1:500), anti-DAT (1:500), anti-dopamine $D_2$ receptor (1:500) and anti-VMAT2 (1:500) primary antibodies as described earlier.[86] In brief, the fixed cells were then blocked in PBS containing 5% bovine serum albumin and 0.01% Tween-20 for half an hour followed by overnight incubation with primary antibodies at 4 °C. The next day the primary antibodies were aspirated and the cells were washed three times with PBS. Cells were further incubated with anti-mouse, anti-goat, or anti-rabbit Alexa 488/Alexa 568 conjugated secondary antibodies (diluted 1:200 in PBS) at room temperature for 2 h followed by washing with PBS. Subsequently the cells were mounted in antifade mounting medium and visualized under a fluorescent microscope (Leica, Germany) equipped with QWin 500 image analysis software. Ten microscopic fields were captured on each slide in a blinded manner. For Mitotracker Deep Red and cytochrome *c* dual labeling, cells after treatment with bulk dopamine and DA NPs were incubated with Mitotracker Deep Red dye (100 nM) and incubated for 1 h at 37 °C. After incubation the dye was aspirated followed by washing with PBS. The cells were then paraformaldehyde fixed and processed for cytochrome *c* immunocytochemistry as discussed above. Representative photomicrographs are included in the article.

*Protein Expression in Cells by Western Blot (WB).* WB of bulk dopamine- or DA NPs-exposed SH-SY5Y cells was carried out as discussed earlier.[84] In brief, cells following exposure were trypsinized and centrifuged at 1000 rpm at room temperature. The cells were lysed using CellLytic buffer (Sigma, USA) supplemented with protease and phosphatase inhibitor cocktail in a shaking water bath incubator maintained at 37 °C. The lysate was centrifuged at 12 000 rpm. Protein in the supernatant was estimated using a Bradford protein estimation kit (Bangalore Genei, India) prior to addition of sample loading buffer. An equal amount of proteins (35 $\mu$g) was loaded on 10% tris-glycine gel and transferred onto a nitrocellulose membrane. Membranes were blocked for 1 h at room temperature in Western blocker (Sigma) followed by overnight incubation with anti-TH, anti-pTH$^{ser31}$, anti-Bcl-2, and anti-Bax antibodies (1:1000). $\beta$-Actin was used as loading control. Membranes were then washed three times with TBST and incubated for 2 h with horseradish peroxidase conjugated secondary antibody. Immunoreactive proteins were detected using a chemiluminescent substrate (Pierce, USA) according to the manufacturer's instructions. Bands were quantified using the Gel Documentation System (Alpha Innotech, USA), and densitometry was performed by AlphaEase FC StandAlone V. 4.0.0 software

***In Vivo* Studies.** *In vivo* studies were carried out in order to study plasma pharmacokinetics of DA NPs, their delivery across the BBB, and restorative potential in a 6-OHDA-induced rat model of PD.

*Animals.* Adult Wistar rats (225 ± 10 g body weight) obtained from the animal breeding colony of Indian Institute of Toxicology Research were used in the current study. These rats were given *ad libitum* water and pellet diet (Hindustan Lever Laboratory Animal Feed, India), and a 12 h light/dark cycle was maintained. All the procedures of animal experimentation were approved by the Institutional Animal Care and Ethical Committee.

*Preparation of the Rat Model of PD through 6-OHDA Lesioning and Administration of NPs.* The rat model of PD was prepared following our earlier study.[86] In brief, rats were

anesthetized with an intraperitoneal injection of a ketamine/xylazine mixture. Each rat received two unilateral stereotaxic injections of freebase 6-OHDA (4 $\mu$g/$\mu$L in 0.2% L-ascorbate saline, 1 $\mu$L/min) in the right medial forebrain bundle of the nigrostriatal pathway following coordinates (in mm with respect to bregma): (i) 3 $\mu$L at anterior posterior (AP) = 4.4, lateral (L) = 1.2, ventral (V) = 7.8; (ii) 2 $\mu$L at AP = 4.0, L = 0.8, V = 8.0.[87] The needle was left *in situ* for an additional 5 min for 6-OHDA diffusion. Rats of the sham group were infused similarly with L-ascorbate saline. To reduce pain, animals were given subcutaneous injections of bupivacaine (2 mg/kg) every 12 h during the first 2 days postsurgery. Three weeks later, lesion efficacy was determined by the number of ipsilateral rotations shown by animals on D-amphetamine challenge (5 mg/kg, ip) as described earlier.[71] Rats who exhibited >6 ipsilateral rotations/min were considered adequately lesioned and used in further study. The animals were randomly divided into the following groups and exposed as per the experimental setup:

Group I (control): normal animals

Group II (sham): L-ascorbate saline lesioned rats

Group III (Les): 6-OHDA-lesioned rats receiving *n*-saline as sham infusion

Group IV (Les + DA NPs-SD): lesioned rats receiving single iv infusion of DA NPs (equivalent to 4.95 mg/kg body weight dopamine)

Group V (Les + DA NPs-DD): lesioned rats receiving two iv infusions of DA NPs (equivalent to 4.95 mg/kg body weight dopamine/injection) on alternate days

Groups VI (Les + PLGA NPs): lesioned rats receiving iv infusion of PLGA NPs

Seven days after last iv injection, rats were subjected to neurobehavioral, neurochemical, and immunohistochemical evaluations.

*Visualization of NPs across the BBB.* Rats of control, sham, and Les groups were given an iv injection of PLGA NPs-FITC (6 mg/kg body weight) suspended in sterile *n*-saline or vehicle alone. After 4 h, the rats were anaesthetized. To demonstrate the presence of fluoresceinylated NPs in the striatal region, the animals were perfused with *n*-saline and paraformaldehyde. The brains were excised and cryopreserved in graded sucrose (10−30%). The perfused brains were then sectioned across the striatum, and the sections were immunostained with anti-TH antibody as discussed later. In order to localize the striatum, photographs were taken at lower magnifications where, below the line of the corpus callosum, the striatum could be easily distinguished.

To show whether infused NPs have crossed the capillary wall, following 4 h of PLGA NPs-FITC iv infusion, the animals were anaesthetised and sacrificed by cervical dislocation. The brains were excised, immediately chilled on dry ice, and transferred to −80 °C. Frozen brains were sectioned across the striatal region and collected on gelatin-coated slides. These sections were further immunostained with anti-endoglin antibody (1:250) to mark the capillaries similarly as discussed later.[23] Suitable secondary antibodies linked to Alexa Fluor-568 were used. These sections were evaluated for location of PLGA NPs-FITC, which crossed the blood capillaries, under a fluorescent microscope.

*NP Visualization and Quantification in the Brain and Peripheral Organs.* Rats were infused with PLGA NPs-FITC (6 mg/kg body weight, iv), anaesthetized, and sacrificed by cervical dislocation after 4 h of treatment. For NP visualization, the brain, kidney, spleen, liver, and heart were excised, immediately chilled on dry ice, and transferred to −80 °C. Sections of 20 $\mu$m thickness were cut using a cryotome (Labcon, Germany). Sections were transferred onto slides and mounted in aqueous mounting media followed by visualization under a fluorescent microscope for FITC signal. The quantification of NPs reaching various brain parts and extra CNS organs was carried out 4 h postinjection following the method of Sundaram *et al.*[88] In brief, 55 mg of various tissues was homogenized in 1 mL of 2% Triton X-100. The homogenate was centrifuged at 3000 rpm for 10 min to remove tissue debris. The supernatant was collected to analyze the amount of PLGA NPs-FITC taken up by the tissue using a spectrofluorometer. An excitation wavelength of 483 nm, emission wavelength of 538 nm, and bandwidths of 3 or 5 nm were used. A similar approach was used for the preparation of standards in tissues. Briefly, similar amounts of area-matched tissues obtained from control animals were spiked with serially diluted stock NP suspensions (0.3−100 $\mu$g/mL) prepared in 2% Triton X-100. The tissues were homogenized and centrifuged, and the supernatant obtained was used to plot standard curves.

*Ultracellular Analysis through TEM.* Localization of DA NPs in SH-SY5Y cells/rat brain regions and ultrastructural changes caused by bulk dopamine and DA NPs following various exposure schedules were studied using TEM.[23] In brief, after exposure to 100 $\mu$g/mL bulk dopamine for 48 h or equivalent DA NPs, SH-SY5Y cells were trypsinized and centrifuged at 1000 rpm to pellet. Animals of sham and 6-OHDA-lesioned group or 6-OHDA-lesioned animals who received a single or double infusion of DA NPs (equivalent to 4.95 mg/kg dopamine/injection) were transcardially perfused with prechilled 1 N saline followed by a 4% paraformaldehyde + 0.2% glutaraldehyde mixture 7 days after the last infusion. Brains were excised, and the striatum and nigra were dissected out and chopped into small pieces (~2 $mm^3$). Both cells and tissues were fixed in 2.5% glutaraldehyde in 0.1 M sodium cacodylate buffer, pH 7.4, at 4 °C for 2 h and overnight, respectively, followed by postfixation in 1% aqueous osmium tetraoxide ($OsO_4$) for 2 h at room temperature. $OsO_4$ was removed, and both cell pellets/tissue pieces were serially dehydrated in graded acetone (15−100%). Cell pellets/tissue pieces were then embedded in an Araldite and dodecenyl succinic anhydride mixture to prepare blocks. These blocks were then baked for 48 h at 65 °C. Ultrathin sections (50−70 nm) were cut with a Leica EM UC7 ultramicrotome and stained with uranyl acetate and lead citrate. Analysis of sections was performed under a TEM (FEI Technai G2spirit twin) equipped with a Gatan digital CCD camera (The Netherlands) at 60 or 80 kV.

**Neurobehavioral Studies.** *Amphetamine-Induced Rotations.* For assessment of circling behavior, rats of sham and lesioned groups were used. Lesioned rats were further assigned to three groups. All these rats were housed individually. D-Amphetamine (5 mg/kg ip) was given, and ipsilateral circling was scored after 30 min for 10 min as reported earlier.[71] Thereafter, animals of the two-lesioned group were given a single or double infusion of DA NPs. Seven days after the last infusion, the amphetamine challenge was repeated. All the scoring was performed in a blinded fashion by an observer unaware of group identity. Data were represented as ipsilateral rotations/min in comparison to sham or to pretreatment score.

*Spontaneous Locomotor Activity (SLA).* An ActiMot detection system (TSE Systems, Bad Homburg, Germany) was used to monitor SLA in rats of sham, lesioned, and lesioned with single or double infusion of DA NPs with minimal observer's bias in the quantification of motility.[89] The locomotor activity was recorded for 5 min and processed by the microcomputer for data analysis. After every trial, the activity chamber was swabbed with ethanol (70%) to eliminate interference due to animal odors. Results were expressed as distance traveled (cm).

*Determination of Dopamine and Metabolites through High-Performance Liquid Chromatography.* Brain striatal levels of dopamine and its metabolites DOPAC and HVA were determined by an HPLC-electrochemical detector system (Waters, Milford, MA, USA) as reported earlier.[90] In brief, rats of various groups (control, sham, lesioned, and control and lesioned with single or double infusion of DA NPs or PLGA NPs) after completion of treatment were anaesthetized as discussed above and sacrificed. The brain striatum was dissected and homogenized in 0.17 M perchloric acid containing 3,4-dihydroxybenzylamine (25 ng/mL) as an internal standard. The homogenate was centrifuged (36000*g*) at 4 °C for 10 min. Then 20 $\mu$L of supernatant was run on HPLC for estimation of dopamine, DOPAC, and HVA. The mobile phase (pH 4.2) consisted of 0.15 M sodium dihydrogen phosphate, 0.25 mM ethylenediaminetetraacetic acid, 1.75 mM sodium octyl sulfate, and 4% methanol. A flow rate of 1.5 mL/min was maintained to separate peaks. The results are expressed as ng/g by tissue weight.

*Dopamine-D2 Receptor Assay.* Radioligand $^3$H-spiperone was used to determine dopamine-D2 receptors in the rat brain striatum as reported earlier.[76] In brief, the crude synaptic membrane was prepared by homogenizing the striatal region in 19 volumes of Tris-HCl buffer (5 mM, pH 7.4) followed by centrifugation at 50000*g* for 15 min at 4 °C. The pellet was

washed twice with the same buffer and finally suspended in Tris-HCl buffer (40 mM, pH 7.4) and stored at −20 °C. Receptor binding was carried out in 1 mL final volume in triplicate. Total binding was estimated using a reaction cocktail composed of Tris-HCl buffer (40 mM, pH 7.4), synaptic membrane protein (200 $\mu$g), and radioligand $^3$H-spiperone ($10^{-9}$ M, specific activity: 18.5 Ci/mmol). For nonspecific binding, dopamine antagonist haloperidol ($10^{-6}$ M) was included in the reaction cocktail. The reaction mixture was incubated for 15 min at 37 °C followed by filtration through glass fiber filter discs (25 mm diameter, 0.3 $\mu$m pore size, Whatman GF/B) using a vacuum manifold. The filters were washed twice, air-dried, and transferred to scintillation vials. Scintillation fluid was added to the vials, and membrane-bound radioactivity was counted using a $\beta$-scintillation counter (Packard, USA) at an efficiency of 30−40% for $^3$H. Specific biding was calculated by subtracting the nonspecific binding from the total binding. The results are expressed as pmol $^3$H-spiperone bound/g protein. In addition to this, receptor affinity ($K_d$) and maximum number of receptor binding sites ($B_{max}$) were analyzed through Scatchard analysis at increasing concentrations of radioligand (1/10 to 10 times the affinity).

*Immunohistochemistry.* In order to examine the effects of DA NPs on striatal and nigral TH expression, immunohistochemical analysis was carried out as per our earlier published method.[71] Seven days after the last infusion of DA NPs, rats ($n$ = 5/group) of sham, 6-OHDA-lesioned, and lesioned + DA NPs-DD were anaesthetized as discussed above and were perfused sequentially with prechilled $n$-saline and 4% paraformaldehyde. The brains were excised, postfixed in 4% paraformaldehyde, and cryopreserved in graded sucrose. Coronal sections (12 $\mu$m) of rat brain striatum and nigral regions were cut using a cryotome (Microm, Germany). Free-floating sections were blocked with 3% normal goat serum, 0.1% Triton X-100, and 0.5% bovine serum albumin for 2 h. Sections were then incubated in mouse anti-TH (1:500) antibody for 24 h at 4 °C followed by three washes with PBS containing Tween-20. These sections were then incubated with anti-mouse peroxidase or Alexa Fluor-488 (1:200) conjugated antibodies for 2 h at room temperature. Color in peroxidase-labeled sections was developed using diaminobenzidine substrate. The sections were transferred to gelatin-coated slides, followed by serial dehydration in graded alcohol and finally in xylene. The sections were then mounted in DPX mountant. Fluorescent labeled sections were mounted in DAPI containing antifade mounting medium (Vectashield, Vector Laboratories, USA) and stored in the dark at 4 °C. Slides were analyzed under a Nikon Eclipse Ti−S inverted fluorescent microscope equipped with a Nikon Digital Sight Ds-Ri1 CCD camera and NIS Elements BR imaging software (Nikon, Japan).

*Striatal and Nigral Protein Expression by Western Blot.* WB was carried out in order to evaluate the effect of DA NP exposure on the brain dopamine system as discussed in our earlier report.[23] In brief, rats of sham, 6-OHDA-lesioned and lesioned + DA NPs-DD groups, 7 days after last infusion, were deeply anesthetized and decapitated, and brains were immediately excised. The striatum of the lesioned side was dissected, weighed, and homogenized in tissue lysis medium (Sigma, USA) supplemented with protease and phosphatase inhibitor cocktail. The homogenate was centrifuged for 15 min at 14000$g$ to remove insoluble material. Protein concentration was determined by the Bradford method kit. A 2× SDS loading buffer (10 mM Tris-HCl buffer pH 6.8, 10% glycerol, 2% sodium dodecyl sulfate, 0.01% bromophenol blue, and 5% $\beta$-mercaptoethanol) was added to the samples followed by boiling for 10 min. A 35 $\mu$g amount of protein was applied to a 10% SDS-polyacrylamide minigel and transferred onto the nitrocellulose membranes. Membranes were then probed with primary antibodies for TH (1:1000) and DAT (1:1000). Detection of primary antibody was done by anti-rabbit secondary antibodies conjugated to horseradish peroxidase (1:5000), and the signals were detected with ECL Western blotting substrate and imaged using VersaDoc (Biorad, Hercules, CA, USA). For level of protein loading, the blots were stripped and reprobed with antibody $\beta$-actin (1:1000). Several exposure times were used to obtain signals in the linear range. Bands were imaged using the Gel Documentation System (Alpha Innotech, USA), and densitometry was performed by AlphaEase FC StandAlone V. 4.0.0 software.

*Estimation of Protein-Bound Quinones (Quinoprotein).* Quinoprotein estimation was carried out as described earlier.[91] In brief, after completion of exposure, 5% lysate was prepared by homogenizing tissues in ice-cold lysis buffer (PBS, pH 7.4, 1% NP-40, 0.5% sodium deoxycholate, and 0.1% sodium dodecyl sulfate + 10 $\mu$g/mL phenylmethylsulfonyl fluoride). The NBT (nitro blue tetrazolium)/glycinate assay was used to determine quinoprotein in the lysate. In brief, 100 $\mu$L of lysate was added to an equal amount of the NBT reagent (0.24 mM NBT in 2 M potassium glycinate, pH 10) followed by incubation at 25 °C for 2 h in the dark with continuous shaking. Absorbance (OD) was measured at 550 nm. The Bradford protein assay kit (Merck, India) was used to measure protein. Bovine serum albumin was used as a standard. Results are expressed as $OD_{550}$/mg protein.

*Histopathology.* Tissue histopathology ($n$ = 5) was carried out in formalin-fixed tissues as described earlier.[92] In brief, kidney, liver, spleen, and heart were extracted, washed in saline, and fixed in 10% buffered formalin for 72 h prior to dehydration in graded ethanol series, with final clearance in xylene. Dehydrated tissues were embedded in paraffin to prepare blocks. These blocks were sequentially sectioned (4−5 $\mu$m), using a microtome (Leica, RM 2155), and subsequently stained with hematoxylin and eosin. Images were taken using a Leica (DFC 295) camera on a Leica microscope.

*Measurement of Hemodynamic Parameters.* Estimation of hemodynamic parameters was performed as described earlier with slight modifications.[93,94] Rats ($n$ = 5) were anaesthetized with urethane (0.625 g/kg, ip; Sigma, USA), and the trachea was cannulized with polyethylene tubing. The left carotid artery was cannulized and catheterized. The catheters were connected to a pressure transducer to record the blood pressure and heart rate. Normal saline, PLGA NPs, DA NPs, and bulk dopamine (200 $\mu$g/kg, positive control) were administered through the cannulated right external jugular vein. Computer-based recording and a data acquisition system (AD Instruments) were used for recording the output signals.

*Co-localization.* Co-localization data were analyzed using ImageJ (National Institutes of Health) employing the JACoP plugin. The statistical test included in the analyses was Mander's co-localization coefficient, showing the percentage of FITC co-localization with Mitotracker Red ($M$ = 1 regarded as perfect correlation).[95]

*Statistics.* Statistical analysis was carried out by using GraphPad InStat statistical analysis software (San Diego, CA, USA). The homogeneity of variance between all the experimental groups was ascertained, and the mean significant difference in the experimental groups was determined using one-way analysis of variance (ANOVA) followed by the Tukey−Kramer *post hoc* multiple comparisons test. $p$-Values less than 0.05 were considered to be statistically significant.

*Conflict of Interest:* The authors declare no competing financial interest.

*Acknowledgment.* We are grateful to the Director of CSIR-IITR, Lucknow, India, for his continuous support in the present work. K.C.G. thanks ICMR, New Delhi, India, for awarding a Distinguished Scientist Chair. This work was supported by the Department of Science and Technology as Woman Scientist and Ramanna Fellow Grant to K.S. and CSIR network project BSC0108 (MedChem) to R.K.C. Technical help of Mr. Punit Khare in flow cytometry analysis and Mr. Jai Shankar and Ms. Nidhi Arjaria in TEM analysis is acknowledged. This is manuscript communication number 3284.

*Supporting Information Available:* Nine supplementary figures. This material is available free of charge *via* the Internet at http://pubs.acs.org.

## REFERENCES AND NOTES

1. Karatas, H.; Aktas, Y.; Gürsoy-Özdemir, Y.; Bodur, E.; Yemişci, M.; Caban, S.; Vural, A.; Pinarbasli, O.; Capan, Y.; Fernandez-Megia, E.; *et al.* A Nanomedicine Transports a Peptide Caspase-3 Inhibitor across the Blood-Brain Barrier and Provides Neuroprotection. *J. Neurosci.* **2009**, *29*, 13761–13769.

2. Yemişci, M.; Gürsoy-Özdemir, Y.; Caban, S.; Bodur, E.; Capan, Y.; Dalkara, T. Transport of a Caspase Inhibitor across the Blood-Brain Barrier by Chitosan Nanoparticles. *Methods Enzymol.* **2012**, *508*, 253–269.
3. Kozlu, S.; Caban, S.; Yerlikaya, F.; Fernandez-Megia, E.; Novoa-Carballal, R.; Riguera, R.; Yemişci, M.; Gürsoy-Özdemir, Y.; Dalkara, T.; Couvreur, P.; *et al*. An Aquaporin 4 Antisense Oligonucleotide Loaded, Brain Targeted Nanoparticulate System Design. *Pharmazie* **2014**, *69*, 340–345.
4. Gazibara, T.; Stankovic, I.; Tomic, A.; Svetel, M.; Tepavcevic, D. K.; Kostic, V. S.; Pekmezovic, T. Validation and Cross-Cultural Adaptation of the Self-Assessment Disability Scale in Patients with Parkinson's Disease in Serbia. *J. Neurol.* **2013**, *260*, 1970–1977.
5. Dauer, W.; Przedborski, S. Parkinson's Disease: Mechanisms and Models. *Neuron* **2003**, *39*, 889–909.
6. Carlsson, T.; Björklund, T. Restoration of the Striatal Dopamine Synthesis for Parkinson's Disease: Viral Vector-Mediated Enzyme Replacement Strategy. *Curr. Gene Ther.* **2007**, *7*, 109–120.
7. Golde, T. E. The Therapeutic Importance of Understanding Mechanisms of Neuronal Cell Death in Neurodegenerative Disease. *Mol. Neurodegener.* **2009**, *4*, 8.
8. Garcia de Yebenes, J.; Fahn, S.; Mena, M. A.; Pardo, B.; Casarejos, M. J. Intracerebroventricular Infusion of Dopamine and Its Agonists in Rodents and Primates. An Experimental Approach to the Treatment of Parkinson's Disease. *ASAIO Trans.* **1988**, *34*, 951–957.
9. Galvan, A.; Floran, B.; Erlij, D.; Aceves, J. Intrapallidal Dopamine Restores Motor Deficits Induced by 6-Hydroxydopamine in the Rat. *J. Neural Transm.* **2001**, *108*, 153–166.
10. Senthilkumar, K. S.; Saravanan, K. S.; Chandra, G.; Sindhu, K. M.; Jayakrishnan, A.; Mohanakumar, K. P. Unilateral Implantation of Dopamine-Loaded Biodegradable Hydrogel in the Striatum Attenuates Motor Abnormalities in the 6-Hydroxydopamine Model of Hemi-Parkinsonism. *Behav. Brain Res.* **2007**, *184*, 11–18.
11. Salat, D.; Tolosa, E. Levodopa in the Treatment of Parkinson's Disease: Current Status and New Developments. *J. Parkinsons Dis.* **2013**, *3*, 255–269.
12. Connolly, B. S.; Lang, A. E. Pharmacological Treatment of Parkinson Disease: A Review. *JAMA, J. Am. Med. Assoc.* **2014**, *311*, 1670–1683.
13. Krishna, R.; Ali, M.; Moustafa, A. A. Effects of Combined MAO-B Inhibitors and Levodopa *vs.* Monotherapy in Parkinson's Disease. *Front. Aging Neurosci.* **2014**, *6*, 180.
14. Kuwabara, H.; Cumming, P.; Yasuhara, Y.; Léger, G. C.; Guttman, M.; Diksic, M.; Evans, A. C.; Gjedde, A. Regional Striatal DOPA Transport and Decarboxylase Activity in Parkinson's Disease. *J. Nucl. Med.* **1995**, *36*, 1226–1231.
15. D'Aurizio, E.; Sozio, P.; Cerasa, L. S.; Vacca, M.; Brunetti, L.; Orlando, G.; Chiavaroli, A.; Kok, R. J.; Hennink, W. E.; Di Stefano, A. Biodegradable Microspheres Loaded with an Anti-Parkinson Prodrug: An *in Vivo* Pharmacokinetic Study. *Mol. Pharmaceutics* **2011**, *8*, 2408–2415.
16. Ren, T.; Yang, X.; Wu, N.; Cai, Y.; Liu, Z.; Yuan, W. Sustained-Release Formulation of Levodopa Methyl Ester/Benserazide for Prolonged Suppressing Dyskinesia Expression in 6-OHDA-Leisoned Rats. *Neurosci. Lett.* **2011**, *502*, 117–122.
17. Wang, A.; Wang, L.; Sun, K.; Liu, W.; Sha, C.; Li, Y. Preparation of Rotigotine-Loaded Microspheres and their Combination Use with L-DOPA to Modify Dyskinesias in 6-OHDA-Lesioned Rats. *Pharm. Res.* **2012**, *29*, 2367–2376.
18. Regnier-Delplace, C.; Thillaye du Boullay, O.; Siepmann, F.; Martin-Vaca, B.; Degrave, N.; Demonchaux, P.; Jentzer, O.; Bourissou, D.; Siepmann, J. PLGA Microparticles with Zero-Order Release of the Labile Anti-Parkinson Drug Apomorphine. *Int. J. Pharm.* **2013**, *443*, 68–79.
19. Wright, B. A.; Waters, C. H. Continuous Dopaminergic Delivery to Minimize Motor Complications in Parkinson's Disease. *Expert Rev. Neurother.* **2013**, *13*, 719–729.
20. Carlsson, T.; Winkler, C.; Burger, C.; Muzyczka, N.; Mandel, R. J.; Cenci, A.; Björklund, A.; Kirik, D. Reversal of Dyskinesias in an Animal Model of Parkinson's Disease by Continuous L-DOPA Delivery Using rAAV Vectors. *Brain* **2005**, *128*, 559–569.
21. Pellicano, C.; Benincasa, D.; Fanciulli, A.; Latino, P.; Giovannelli, M.; Pontieri, F. E. The Impact of Extended Release Dopamine Agonists on Prescribing Patterns for Therapy of Early Parkinson's Disease: An Observational Study. *Eur. J. Med. Res.* **2013**, 18–60.
22. Vergara-Aragón, P.; Domínguez-Marrufo, L. E.; Ibarra-Guerrero, P.; Hernandez-Ramírez, H.; Hernández-Téllez, B.; López-Martínez, I. E.; Sánchez-Cervantes, I.; Santiago-Jacinto, P.; García-Macedo, J. A.; Valverde-Aguilar, G.; *et al.* $TiO_2$-Dopamine Complex Implanted Unilaterally in the Caudate Nucleus Improves Motor Activity and Behavior Function of Rats with Induced Hemiparkinsonism. *Proc. West Pharmacol. Soc.* **2011**, *54*, 15–20.
23. Tiwari, S. K.; Agarwal, S.; Seth, B.; Yadav, A.; Nair, S.; Bhatnagar, P.; Karmakar, M.; Kumari, M.; Chauhan, L. K. S.; Patel, D. K.; *et al*. Curcumin-Loaded Nanoparticles Potently Induce Adult Neurogenesis and Reverse Cognitive Deficits in Alzheimer's Disease Model via Canonical Wnt/$\beta$-Catenin Pathway. *ACS Nano* **2014**, *8*, 76–103.
24. Jose, S.; Sowmya, S.; Cinu, T. A.; Aleykutty, N. A.; Thomas, S.; Souto, E. B. Surface Modified PLGA Nanoparticles for Brain Targeting of Bacoside-A. *Eur. J. Pharm. Sci.* **2014**, *63*, 29–35.
25. Tiwari, M. N.; Agarwal, S.; Bhatnagar, P.; Singhal, N. K.; Tiwari, S. K.; Kumar, P.; Chauhan, L. K.; Patel, D. K.; Chaturvedi, R. K.; Singh, M. P.; *et al*. Nicotine-Encapsulated Poly(lactic-co-glycolic) Acid Nanoparticles Improve Neuroprotective Efficacy against MPTP-Induced Parkinsonism. *Free Radical Biol. Med.* **2013**, *65*, 704–718.
26. Hu, K.; Shi, Y.; Jiang, W.; Han, J.; Huang, S.; Jiang, X. Lactoferrin Conjugated PEG-PLGA Nanoparticles for Brain Delivery: Preparation, Characterization and Efficacy in Parkinson's Disease. *Int. J. Pharm.* **2011**, *415*, 273–283.
27. Herrán, E.; Requejo, C.; Ruiz-Ortega, J. A.; Aristieta, A.; Igartua, M.; Bengoetxea, H.; Ugedo, L.; Pedraz, J. L.; Lafuente, J. V.; Hernández, R. M. Increased Antiparkinson Efficacy of the Combined Administration of VEGF- and GDNF-Loaded Nanospheres in a Partial Lesion Model of Parkinson's Disease. *Int. J. Nanomed.* **2014**, *9*, 2677–2687.
28. Bissonnette, B.; Sims, C. Resuscitation Agents. *Pediatr. Anesth.-Basic Principles, State Art, Future* **2011**, 552–570.
29. Lankveld, D. P.; Oomen, A. G.; Krystek, P.; Neigh, A.; Troost-de Jong, A.; Noorlander, C. W.; Van Eijkeren, J. C.; Geertsma, R. E.; De Jong, W. H. The Kinetics of the Tissue Distribution of Silver Nanoparticles of Different Sizes. *Biomaterials* **2010**, *31*, 8350–8361.
30. Unsoy, G.; Khodadust, R.; Yalcin, S.; Mutlu, P.; Gunduz, U. Synthesis of Doxorubicin Loaded Magnetic Chitosan Nanoparticles for pH Responsive Targeted Drug Delivery. *Eur. J. Pharm. Sci.* **2014**, *62*, 243–250.
31. Zolnik, B. S.; Burgess, D. J. Effect of Acidic pH on PLGA Microsphere Degradation and Release. *J. Controlled Release* **2007**, *122*, 338–434.
32. Faisant, N.; Siepmann, J.; Benoit, J. P. PLGA-Based Microparticles: Elucidation of Mechanisms and a New, Simple Mathematical Model Quantifying Drug Release. *Eur. J. Pharm. Sci.* **2002**, *15*, 355–366.
33. Lazzari, S.; Moscatelli, D.; Codari, F.; Salmona, M.; Morbidelli, M.; Diomede, L. Colloidal Stability of Polymeric Nanoparticles in Biological Fluids. *J. Nanopart. Res.* **2012**, *14*, 920–929.
34. Wang, H.; Zhao, Y.; Wua, Y.; Hub, Y.; Nan, K.; Nie, G.; Chen, H. Enhanced Anti-Tumor Efficacy by Co-delivery of Doxorubicin and Paclitaxel with Amphiphilic Methoxy PEG-PLGA Copolymer Nanoparticles. *Biomaterials* **2011**, *32*, 8281–8290.
35. Nevesa, J.; Amijic, M.; Bahiab, M. F.; Sarmento, B. Assessing the Physical-Chemical Properties and Stability of Dapivirine-Loaded Polymeric Nanoparticles. *Int. J. Pharm.* **2013**, *456*, 307–314.
36. Bisaglia, M.; Mammi, S.; Bubacco, L. Kinetic and Structural Analysis of the Early Oxidation Products of Dopamine: Analysis of the Interactions with Alpha-Synuclein. *J. Biol. Chem.* **2007**, *282*, 15597–15605.

37. Witkovsky, P.; Patel, J. C.; Lee, C. R.; Rice, M. E. Immunocytochemical Identification of Proteins Involved in Dopamine Release from the Somatodendritic Compartment of Nigral Dopaminergic Neurons. *Neuroscience* **2009**, *164*, 488–496.
38. Sotnikova, T. D.; Beaulieu, J. M.; Gainetdinov, R. R.; Caron, M. G. Molecular Biology, Pharmacology and Functional Role of the Plasma Membrane Dopamine Transporter. *CNS Neurol. Disord. Drug Targets* **2006**, *5*, 45–56.
39. Nirenberg, M. J.; Vaughan, R. A.; Uhl, G. R.; Kuhar, M. J.; Pickell, V. M. The Dopamine Transporter Is Localized to Dendritic and Axonal Plasma Membranes of Nigrostriatal Dopaminergic Neurons. *J. Neurosci.* **1996**, *76*, 436–447.
40. Eriksen, J.; Rasmussen, S. G. F.; Rasmussen, T. N.; Vaegter, C. B.; Cha, J. H.; Zou, M.; Newman, A. H.; Gether, U. Visualization of Dopamine Transporter Trafficking in Live Neurons by Use of Fluorescent Cocaine Analogs. *J. Neurosci.* **2009**, *29*, 6794–6808.
41. Pickel, V. M.; Chan, J.; Nirenberg, M. J. Region-Specific Targeting of Dopamine D2-Receptors and Somatodendritic Vesicular Monoamine Transporter 2 (VMAT2) within Ventral Tegmental Area Subdivisions. *Synapse* **2002**, *45*, 113–124.
42. Xu, P.; Gullotti, E.; Tong, L.; Highley, C. B.; Errabelli, D. R.; Hasan, T.; Cheng, J. X.; Kohane, D. S.; Ye, Y. Intracellular Drug Delivery by Poly(lactic-co-glycolic acid) Nanoparticles, Revisited. *Mol. Pharmaceutics* **2009**, *6*, 190–201.
43. Park, I. K.; Lasiene, J.; Chou, S. H.; Horner, P. J.; Pun, S. H. Neuron-Specific Delivery of Nucleic Acids Mediated by Tet1-Modified Poly(ethylenimine). *J. Gene Med.* **2007**, *9*, 691–702.
44. Singhal, A.; Morris, V. B.; Labhasetwar, V.; Ghorpade, A. Nanoparticle-Mediated Catalase Delivery Protects Human Neurons from Oxidative Stress. *Cell Death Dis.* **2013**, *4*, e903.
45. Jiang, Y.; Pei, L.; Li, S.; Wang, M.; Liu, F. Extracellular Dopamine Induces the Oxidative Toxicity of SH-SY5Y Cells. *Synapse* **2008**, *62*, 797–803.
46. Asanuma, M.; Miyazaki, I.; Ogawa, N. Dopamine- or L-DOPA-Induced Neurotoxicity: The Role of Dopamine Quinone Formation and Tyrosinase in a Model of Parkinson's Disease. *Neurotox. Res.* **2003**, *5*, 165–176.
47. Asanuma, M.; Miyazaki, I.; Diaz-Corrales, F. J.; Ogawa, N. Quinone Formation as Dopaminergic Neuron-Specific Oxidative Stress in the Pathogenesis of Sporadic Parkinson's Disease and Neurotoxin-Induced Parkinsonism. *Acta Med. Okayama* **2004**, *58*, 221–233.
48. Kura, A. U.; Ain, N. M.; Hussein, M. Z.; Fakurazi, S.; Hussein-Al-Ali, S. H. Toxicity and Metabolism of Layered Double Hydroxide Intercalated with Levodopa in a Parkinson's Disease Model. *Int. J. Mol. Sci.* **2014**, *15*, 5916–5927.
49. Tan, J. M.; Foo, J. B.; Fakurazi, S.; Hussein, M. Z. Release Behaviour and Toxicity Evaluation of Levodopa from Carboxylated Single-Walled Carbon Nanotubes. *Beilstein J. Nanotechnol.* **2015**, *6*, 243–253.
50. Ham, A.; Lee, S. J.; Shin, J.; Kim, K. H.; Mar, W. Regulatory Effects of Costunolide on Dopamine Metabolism-Associated Genes Inhibit Dopamine-Induced Apoptosis in Human Dopaminergic SH-SY5Y Cells. *Neurosci. Lett.* **2012**, *507*, 101–105.
51. Koshimura, K.; Tanaka, J.; Murakami, Y.; Kato, Y. Effects of Dopamine and L-DOPA on Survival of PC12 Cells. *J. Neurosci Res.* **2000**, *62*, 112–119.
52. Kawashima, T.; Ohkubo, K.; Fukuzumi, S. Radical Scavenging Reactivity of Catecholamine Neurotransmitters and the Inhibition Effect for DNA Cleavage. *J. Phys. Chem. B* **2010**, *114*, 675–680.
53. O'Keeffe, G. C.; Barker, R. A.; Caldwell, M. A. Dopaminergic Modulation of Neurogenesis in the Subventricular Zone of the Adult Brain. *Cell Cycle* **2009**, *8*, 2888–2894.
54. O'Keeffe, G. C.; Tyers, P.; Aarsland, D.; Dalley, J. W.; Barker, R. A.; Caldwell, M. A. Dopamine-Induced Proliferation of Adult Neural Precursor Cells in the Mammalian Subventricular Zone is Mediated through EGF. *Proc. Natl. Acad. Sci. U.S.A.* **2009**, *106*, 8754–8759.
55. Höglinger, G.; Rizk, P.; Muriel, M. P.; Duyckaerts, C.; Oertel, W. H.; Caille, I.; Hirsch, E. C. Dopamine Depletion Impairs Precursor Cell Proliferation in Parkinson Disease. *Nat. Neurosci.* **2004**, *7*, 726–735.
56. Chaturvedi, R. K.; Shukla, S.; Seth, K.; Agrawal, A. K. Zuckerkandl's Organ Improves Long-Term Survival and Function of Neural Stem Cell Derived Dopaminergic Neurons in Parkinsonian Rats. *Exp. Neurol.* **2008**, *210*, 608–623.
57. Bisaglia, M.; Soriano, M. E.; Arduini, I.; Mammi, S.; Bubacco, L. Molecular Characterization of Dopamine-Derived Quinones Reactivity toward NADH and Glutathione: Implications for Mitochondrial Dysfunction in Parkinson Disease. *Biochim. Biophys. Acta* **2010**, *1802*, 699–706.
58. Belluzzi, E.; Bisaglia, M.; Lazzarini, E.; Tabares, L. C.; Beltramini, M.; Bubacco, L. Human SOD2 Modification by Dopamine Quinones Affects Enzymatic Activity by Promoting Its Aggregation: Possible Implications for Parkinson's Disease. *PLoS One* **2012**, *7*, e38026.
59. Vermeer, L. M.; Florang, V. R.; Doorn, J. A. Catechol and Aldehyde Moieties of 3,4-Dihydroxyphenylacetaldehyde Contribute to Tyrosine Hydroxylase Inhibition and Neurotoxicity. *Brain Res.* **2012**, *1474*, 100–109.
60. Brunelle, J. K.; Letai, A. Control of Mitochondrial Apoptosis by the Bcl-2 Family. *J. Cell Sci.* **2009**, *122*, 437–441.
61. D'Herde, K.; De Prest, B.; Mussche, S.; Schotte, P.; Beyaert, R.; Coster, R. V.; Roels, F. Ultrastructural Localization of Cytochrome C in Apoptosis Demonstrates Mitochondrial Heterogeneity. *Cell Death Di*X*er.* **2000**, *7*, 331–337.
62. Tait, S. W.; Green, D. R. Mitochondria and Cell Death: Outer Membrane Permeabilization and Beyond. *Nat. Rev. Mol. Cell Biol.* **2010**, *11*, 621–632.
63. Kang, C. D.; Jang, J. H.; Kim, K. W.; Lee, H. J.; Jeong, C. S.; Kim, C. M.; Kim, S. H.; Chung, B. S. Activation of c-jun N-Terminal Kinase/Stress-Activated Protein Kinase and the Decreased Ratio of Bcl-2 to Bax Are Associated with the Auto-Oxidized Dopamine-Induced Apoptosis in PC12 Cells. *Neurosci. Lett.* **1998**, *256*, 37–40.
64. van der Heide, L. P.; Smidt, M. P. The BCL2 Code to Dopaminergic Development and Parkinson's Disease. *Trends Mol. Med.* **2013**, *19*, 211–216.
65. Wang, D. B.; Kinoshita, C.; Kinoshita, Y.; Morrison, R. S. p53 and Mitochondrial Function in Neurons. *Biochim. Biophys. Acta* **2014**, *1842*, 1186–1197.
66. Jeon, S. M.; Cheon, S. M.; Bae, H. R.; Kim, J. W.; Kim, S. U. Selective Susceptibility of Human Dopaminergic Neural Stem Cells to Dopamine-Induced Apoptosis. *Exp. Neurobiol.* **2010**, *19*, 155–164.
67. Parrot, S.; Neuzeret, P. C.; Denoroy, L. A Rapid and Sensitive Method for the Analysis of Brain Monoamine Neurotransmitters Using Ultra-fast Liquidchromatography Coupled to Electrochemical Detection. *J. Chromatogr. B Analyt. Technol. Biomed. Life Sci.* **2011**, *879*, 3871–3878.
68. Gambaryan, P. Y.; Kondrasheva, I. G.; Severin, E. S.; Guseva, A. A.; Kamensky, A. A. Increasing the Efficiency of Parkinson's Disease Treatment Using a Poly(lactic-co-glycolic acid) (PLGA) Based L-DOPA Delivery System. *Exp. Neurobiol.* **2014**, *23*, 246–252.
69. Trapani, A.; De Giglio, E.; Cafagna, D.; Denora, N.; Agrimi, G.; Cassano, T.; Gaetani, S.; Cuomo, V.; Trapani, G. Characterization and Evaluation of Chitosan Nanoparticles for Dopamine Brain Delivery. *Int. J. Pharm.* **2011**, *419*, 296–307.
70. Asanuma, M.; Miyazaki, I.; Murakami, S.; Diaz-Corrales, F. J.; Ogawa, N. Striatal Astrocytes Act as a Reservoir for L-DOPA. *PLoS One* **2014**, *9*, e106362.
71. Shukla, S.; Chaturvedi, R. K.; Seth, K.; Roy, N. S.; Agrawal, A. K. Enhanced Survival and Function of Neural Stem Cells-Derived Dopaminergic Neurons under Influence of Olfactory Ensheathing Cells in Parkinsonian Rats. *J. Neurochem.* **2009**, *109*, 436–451.
72. Woiciechowsky, C.; Guilarte, T. R.; May, C. H.; Vesper, J.; Wagner, H. N., Jr.; Vogel, S. Intrastriatal Dopamine Infusion Reverses Compensatory Increases in D2-Dopamine Receptors in the 6-OHDA Lesioned Rat. *Neurodegeneration* **1995**, *4*, 161–169.

73. Wei, W.; Li, L.; Yu, G.; Ding, S.; Li, C.; Zhou, F. M. Supersensitive Presynaptic Dopamine D2 Receptor Inhibition of the Striatopallidal Projection in Nigrostriatal Dopamine-Deficient Mice. *J. Neurophysiol.* **2013**, *110*, 2203–2216.
74. Scherfler, C.; Khan, N. L.; Pavese, N.; Lees, A. J.; Quinn, N. P.; Brooks, D. J.; Piccini, P. P. Upregulation of Dopamine D2 Receptors in Dopaminergic Drug-Naive Patients with Parkin Gene Mutations. *Mov. Disord.* **2006**, *21*, 783–788.
75. Sahin, G.; Thompson, L. H.; Lavisse, S.; Ozgur, M.; Rbah-Vidal, L.; Dollé, F.; Hantraye, P.; Kirik, D. Differential Dopamine Receptor Occupancy Underlies L-DOPA-Induced Dyskinesia in a Rat Model of Parkinson's Disease. *PLoS One* **2014**, *9*, e90759.
76. Chaturvedi, R. K.; Shukla, S.; Seth, K.; Agrawal, A. K. Nerve Growth Factor Increases Survival of Dopaminergic Graft, Rescue Nigral Dopaminergic Neurons and Restores Functional Deficits in Rat Model of Parkinson's Disease. *Neurosci. Lett.* **2006**, *398*, 44–49.
77. Yang, X.; Zheng, R.; Cai, Y.; Liao, M.; Yuan, W.; Liu, Z. Controlled-Release Levodopa Methyl Ester/Benserazide-Loaded Nanoparticles Ameliorate Levodopa-Induced Dyskinesia in Rats. *Int. J. Nanomedicine* **2012**, *7*, 2077–2086.
78. Wang, N.; Wang, Y.; Yu, G.; Yuan, C.; Ma, J. Quinoprotein Adducts Accumulate in the Substantia Nigra of Aged Rats and Correlate with Dopamine-Induced Toxicity in SH-SY5Y Cells. *Neurochem. Res.* **2011**, *36*, 2169–2175.
79. Lach, B.; Grimes, D.; Benoit, B.; Janda, A. M. Caudate Nucleus Pathology in Parkinson's Disease: Ultrastructural and Biochemical Findings in Biopsy Material. *Acta Neuropathol.* **1992**, *83*, 352–360.
80. Gutierrez-Valdez, A. L.; Anaya-Martínez, V.; Ordoñez-Librado, J. L.; García-Ruiz, R.; Torres-Esquivel, C.; Moreno-Rivera, M.; Sánchez-Betancourt, J.; Montiel-Flores, E.; Avila-Costa, M. R. Effect of Chronic L-Dopa or Melatonin Treatments after Dopamine Deafferentation in Rats: Dyskinesia, Motor Performance, and Cytological Analysis. *ISRN Neurol.* **2012**, *2012*, e360379.
81. Shin, M.; Kim, H. K.; Lee, H. Dopamine-Loaded Poly(D,L-lactic-co-glycolic acid) Microspheres: New Strategy for Encapsulating Small Hydrophilic Drugs with High Efficiency. *Biotechnol. Prog.* **2014**, *30*, 215–223.
82. Swami, A.; Aggarwal, A.; Pathak, A.; Patnaik, S.; Kumar, P.; Singh, Y.; Gupta, K. C. Imidazolyl-Pei Modified Nanoparticles for Enhanced Gene Delivery. *Int. J. Pharm.* **2007**, *335*, 180–192.
83. Wang, F.; Franco, R.; Skotak, M.; Hu, G.; Chandra, N. Mechanical Stretch Exacerbates the Cell Death in SH-SY5Y Cells Exposed to Paraquat: Mitochondrial Dysfunction and Oxidative Stress. *Neurotoxicology* **2014**, *14*, 54–63.
84. Shukla, A.; Mohapatra, T. M.; Parmar, D.; Seth, K. Neuroprotective Potentials of Neurotrophin Rich Olfactory Ensheathing Cell's Conditioned Media against 6OHDA-Induced Oxidative Damage. *Free Radical Res.* **2014**, *48*, 560–571.
85. Shukla, A.; Mohapatra, T. M.; Agrawal, A. K.; Parmar, D.; Seth, K. Salsolinol Induced Apoptotic Changes in Neural Stem Cells: Amelioration by Neurotrophin Support. *Neurotoxicology* **2013**, *35*, 50–61.
86. Agrawal, A. K.; Shukla, S.; Chaturvedi, R. K.; Seth, K.; Srivastava, N.; Ahmad, A.; Seth, P. K. Olfactory Ensheathing Cell Transplantation Restores Functional Deficits in Rat Model of Parkinson's Disease: A Cotransplantation Approach with Fetal Ventral Mesencephalic Cells. *Neurobiol. Dis.* **2004**, *16*, 516–526.
87. Paxinos, G.; Watson, C. *The Rat Brain in Stereotaxic Coordinates*, 4th ed; Academic Press: CA, 1998.
88. Sundaram, S.; Roy, S. K.; Ambati, B. K.; Kompella, U. B. Surface-Functionalized Nanoparticles for Targeted Gene Delivery across Nasal Respiratory Epithelium. *FASEB J.* **2009**, *23*, 3752–3765.
89. Yadav, R. S.; Sankhwar, M. L.; Shukla, R. K.; Chandra, R.; Pant, A. B.; Islam, F.; Khanna, V. K. Attenuation of Arsenic Neurotoxicity by Curcumin in Rats. *Toxicol. Appl. Pharmacol.* **2009**, *240*, 367–376.
90. Wood, P. L.; Kim, H. S.; Marien, M. R. Intracerebral Dialysis: Direct Evidence for the Utility of 3-MT Measurements as an Index of Dopamine Release. *Life Sci.* **1987**, *41*, 1–5.
91. Miyazaki, I.; Asanuma, M.; Kikkawa, Y.; Takeshima, M.; Murakami, S.; Miyoshi, K.; Sogawa, N.; Kita, T. Astrocyte-Derived Metallothionein Protects Dopaminergic Neurons from Dopamine Quinone Toxicity. *Glia* **2011**, *59*, 435–451.
92. Panigrahi, G.; Tiwari, S.; Ansari, K. M.; Chaturvedi, R. K.; Khanna, V. K.; Chaudhari, B. P.; Vashistha, V. M.; Raisuddin, S.; Das, M. Association between Children Death and Consumption of Cassia occidentalis Seeds: Clinical and Experimental Investigations. *Food Chem. Toxicol.* **2014**, *67*, 236–248.
93. Zhu, Y. Z.; Zhu, Y. C.; Li, J.; Schäfer, H.; Schmidt, W.; Yao, T.; Unger, T. Effects of Losartan on Haemodynamic Parameters and Angiotensin Receptor mRNA Levels in Rat Heart after Myocardial Infarction. *J. Renin Angiotensin Aldosterone Syst.* **2000**, *1*, 257–262.
94. Perez-Olea, J.; Quevedo, M.; Silva, R. Enhancement of Blood Pressure Response to Dopamine by Angiotensin II. *Hypertension* **1981**, *3*, 138–141.
95. Midgley, A. C.; Mathew, R.; Hallett, M. B.; Clayton, A.; Bowen, T.; Phillips, A. O.; Steadman, R. Transforming Growth Factor-$\beta$1 (TGF-$\beta$1)-Stimulated Fibroblast to Myofibroblast Differentiation Is Mediated by Hyaluronan (HA)-Facilitated Epidermal Growth Factor Receptor (EGFR) and CD44 Co-localization in Lipid Rafts. *J. Biol. Chem.* **2013**, *288*, 14824–14838.